Factors Affecting the Electronic Ground State of Low-Spin Iron(III) Porphyrin Complexes

Takahisa Ikeue,[†] Yoshiki Ohgo,[†] Takashi Saitoh,[‡] Tatsuya Yamaguchi,[†] and Mikio Nakamura*[†,‡]

Department of Chemistry, Toho University School of Medicine, Omorinishi, Ota-ku, Tokyo 143-8540, and Division of Biomolecular Science, Graduate School of Science, Toho University, Funabashi, Chiba 274-8510

Received December 18, 2000

To determine the factors affecting the ground-state electron configuration of low-spin Fe(III) porphyrin complexes, we have examined the ^{1}H NMR, ^{13}C NMR, and EPR spectra of a series of low-spin bis-ligated Fe(III) porphyrin complexes $[Fe(Por)L_2]^{\pm}$, in which the positions of porphyrin substituents and the coordination ability of axial ligands are different. The seven porphyrins used in this study are *meso*-tetraalkylporphyrins (TRP: R is propyl, cyclopropyl, or isopropyl), *meso*-tetraphenylporphyrin (TPP), *meso*-tetrakis(2,3,4,5,6-pentafluorophenyl)porphyrin, and 5,10,15,20-tetraphenyl-2,3,7,8,12,13,17,18-octaalkylporphyrins (ORTPP: R is methyl or ethyl). The porphyrin cores of TRP are more or less S_4-ruffled depending on the bulkiness of the alkyl substituents, while those of ORTPP are highly S_4-saddled. Three types of axial ligands are examined which have the following characteristics in ligand field theory: they are (i) strong σ-donating imidazole (HIm), (ii) strong σ-donating and weak π-accepting cyanide (CN^-), and (iii) weak σ-donating and strong π-accepting *tert*-butyl isocyanide (^{t}BuNC). In the case of the bis(HIm) complexes, only the isopropyl complex, $[Fe(T^iPrP)(HIm)_2]^+$, has shown the less common $(d_{xz}, d_{yz})^4(d_{xy})^1$ ground state; the other six complexes have exhibited the common $(d_{xy})^2(d_{xz}, d_{yz})^3$ ground state. When the axial imidazole is replaced by cyanide, even the propyl and cyclopropyl complexes have shown the $(d_{xz}, d_{yz})^4(d_{xy})^1$ ground state; the TPP and ORTPP complexes have still maintained the common $(d_{xy})^2(d_{xz}, d_{yz})^3$ ground state. In the case of the bis(^{t}BuNC) complexes, all the complexes have shown the $(d_{xz}, d_{yz})^4(d_{xy})^1$ ground state. However, the contribution of the $(d_{xz}, d_{yz})^4(d_{xy})^1$ state to the electronic ground state differs from complex to complex; the $(d_{xz}, d_{yz})^4(d_{xy})^1$ contribution is the largest in $[Fe(T^iPrP)(^tBuNC)_2]^+$ and the smallest in $[Fe(OETPPP)(^tBuNC)_2]^+$. We have then examined the electronic ground state of low-spin $[Fe(OEP)(^tBuNC)_2]^+$ and $[Fe(ProtoIXMe_2)(^tBuNC)_2]^+$; OEP and ProtoIXMe$_2$ represent 2,3,7,8,12,13,17,18-octaethylporphyrin and protoporphyrin-IX dimethyl ester, respectively. These porphyrins have a_{1u} HOMO in contrast to the other seven porphyrins that have a_{2u} HOMO. The ^{13}C NMR and EPR studies have revealed that the contribution of the $(d_{xz}, d_{yz})^4(d_{xy})^1$ state in these complexes is as small as that in $[Fe(OETPP)(^tBuNC)_2]^+$. On the basis of these results, we have concluded that the low-spin iron(III) porphyrins that have (i) strong axial ligands, (ii) highly saddle shaped porphyrin rings, (iii) porphyrins with a_{1u} HOMO, and (iv) electron withdrawing substituents at the *meso* positions tend to maintain the common $(d_{xy})^2(d_{xz}, d_{yz})^3$ ground state.

Introduction

Low-spin Fe(III) porphyrin complexes carrying two axial ligands usually have the $(d_{xy})^2(d_{xz}, d_{yz})^3$ ground state.[1] However, recent studies have revealed that some low-spin complexes tend to adopt the less common $(d_{xz}, d_{yz})^4(d_{xy})^1$ ground state if one of the following conditions is satisfied: (i) the axial ligands that are both weak σ-donors and strong π-acceptors such as *tert*-butyl isocyanide (^{t}BuNC) and 4-cyanopyridine (4-CNPy)[1−10] and (ii) the porphyrin rings that are strongly S_4-ruffled such as *meso*-tetraisopropylporphyrin, *meso*-tetramethylchiroporphyrin,

* To whom correspondence should be addressed. E-mail: mnakamu@med.toho-u.ac.jp.

† Toho University School of Medicine.

‡ Graduate School of Science, Toho University.

(1) (a) Walker, F. A. Paramagnetic Molecules. In *Biological Magnetic Resonance*; Berliner, L. J., Reuben, J., Eds.; Plenum Press: New York, 1993; Volume 12, pp 133−274. (b) Walker, F. A. In *The Porphyrin Handbook*; Kadish, K. M., Smith, K. M., Guilard, R., Eds.; Academic Press: San Diego, 2000; Vol. 5, Chapter 36, pp 81−183.

(2) Simonneaux, G.; Hindre, F.; Le Plouzennec, M. *Inorg. Chem*. **1989**, *28*, 823−825.

(3) Safo, M. K.; Gupta, G. P.; Watson, C. T.; Simonis, U.; Walker, F. A.; Scheidt, W. R. *J. Am. Chem. Soc*. **1992**, *114*, 7066−7075.

(4) Safo, M. K.; Walker F. A.; Raitsimring, A. M.; Walters, W. P.; Dolata, D. P.; Debrunner, P. G.; Scheidt, W. R. *J. Am. Chem. Soc.* **1994**, *116*, 7760−7770.

(5) Cheesman, M. R.; Walker, F. A. *J. Am. Chem. Soc*. **1996**, *118*, 7373−7380.

(6) Walker, F. A.; Nasri, H.; Turowska-Tyrk, I.; Mohanrao, K.; Watson, C. T.; Shokhirev, N. V.; Debrunner, P. G.; Scheidt, W. R. *J. Am. Chem. Soc*. **1996**, *118*, 12109−12118.

(7) Safo, M. K.; Marlys, J. M.; Walker F. A.; Debrunner, P. G.; Scheidt, W. R. *J. Am. Chem. Soc*. **1997**, *119*, 9438−9448.

(8) Pilard, M.-A.; Guillemot, M.; Toupet, L.; Jordanov, J.; Simonneaux, G. *Inorg. Chem.* **1997**, *36*, 6307−6314.

(9) Geze, C.; Legrand, N., Bondon, A., Simonneaux, G. *Inorg. Chim. Acta* **1992**, *195*, 73−76.

(10) Abbreviations. ORTPP (R = M or E): dianion of 2,3,7,8,12,13,17,18-octaalkyl-5, 10, 15, 20-tetraphenylporphyrin where R is methyl (M) or ethyl (E). OEP: dianion of 2,3,7,8,12,13,17,18-octaethylporphyrin. THP: dianion of porphine. TRP (R = ^{i}Pr, ^{c}Pr, or ^{n}Pr): dianion of *meso*-tetraalkylporphyrin where R is isopropyl (^{i}Pr), cyclopropyl (^{c}Pr), or propyl (^{n}Pr). TArP, TPP, F_{20}-TPP, TCHP, and TMCP: dianions of *meso*-tetraarylpoprhyrin, *meso*-tetraphenylporphyrin, *meso*-tetrakis(2,3,4,5,6-pentafluorophenyl)porphyrin, *meso*-tetracyclohexylporphyrin, and *meso*-tetramethylchiroporphyrin. ProtoIXMe$_2$: dianion of protoporphyrin IX dimethyl ester. ^{t}BuNC: *tert*-butyl isocyanide. Him: imidazole. 4-CNPy: 4-cyanopyridine. 3-PhPy: 3-phenylpyridine.

10.1021/ic001412b CCC: $20.00
Published on Web 06/08/2001

and *meso*-tetracyclohexylporphyrin.[11−17] The weak crystal field of axial ligands can place the d_{xz}, d_{yz} orbitals at lower energy than d_{xy}, resulting in the formation of the $(d_{xz}, d_{yz})^4(d_{xy})^1$ ground state.[7] The S_4-ruffling of the porphyrin core weakens the $3e_g$(porphyrin)−d_π(iron)[13] and strengthens the a_{2u}(porphyrin)−d_{xy}(iron) interactions.[4] The former stabilizes the iron d_π orbitals and the latter destabilizes the iron d_{xy} orbital, resulting in the stabilization of the $(d_{xz}, d_{yz})^4(d_{xy})^1$ state relative to the $(d_{xy})^2(d_{xz}, d_{yz})^3$ state. As the S_4-ruffling of the porphyrin core increases, the $(d_{xz}, d_{yz})^4(d_{xy})^1$ state is further stabilized. Thus, in the case of the isopropyl complexes, $[Fe(T^iPrP)L_2]^{\pm}$, the $(d_{xz}, d_{yz})^4(d_{xy})^1$ ground state is maintained in the wide range of axial ligands with different coordination ability, i.e., from the very weak ligands such as 4-CNPy to the much stronger ligands such as Py, 3-MePy, 4-NMe_2Py, 2-MeIm, and HIm.[18] Then, the question arises as to how the electron configuration is affected by the deformation mode of porphyrin ring; several deformation modes have been observed including ruffling, saddling, doming, and waving.[19,20] The study on the effect of deformation mode on the heme properties must be very important since the recent research done by Shelnutt and co-workers have revealed that the nonplanar distortions of porphyrins are frequently observed in naturally occurring heme proteins;[21,22] the hemes in cytochromes c, for example, are highly ruffled, while those in peroxidases are mainly saddled.[23,24] We have chosen the low-spin Fe(III) complexes of OMTPP and OETPP as the models for saddle shaped complexes, because the porphyrin rings in OMTPP and OETPP complexes always show the strongly S_4-saddled structure.[25−28] In this paper, we report the ^{1}H NMR, ^{13}C NMR, and EPR spectroscopic results of the low-spin Fe(III) complexes with saddle shaped porphyrin rings such as $[Fe(ORTPP)(HIm)_2]^+$, $[Fe(ORTPP)(CN)_2]^-$, and $[Fe(ORTPP)(^tBuNC)_2]^+$, and compare the spectroscopic results with those of the ruffle shaped complexes such as $[Fe(TRP)(HIm)_2]^+$, $[Fe(TRP)(CN)_2]^-$, and $[Fe(TRP)(^tBuNC)_2]^+$ (R = ^{n}Pr, ^{c}Pr, or ^{i}Pr); although the X-ray crystallographic results of the low-spin $[Fe(TRP)L_2]^+$ (L = HIm, CN^-, or ^{t}BuNC) complexes have not been reported, the porphyrin rings in *meso*-tetraalkylporphyrinates such as $[Ni(T^iPrP)]$,[29] $[Fe(T^iPrP)Cl]$,[30] $[Fe(TMCP)Cl]$,[31] $[Ni(TCHP)]$,[32] $[Fe(T^nPrP)Cl]$,[33] $[Fe(TEtP)(THF)_2]^+$,[34] and $[Fe(T^iPrP)(THF)_2]^+$[35] are known to be ruffled. In the case of $[Fe(T^iPrP)(THF)_2]^+$, the deviations of the *meso* carbon atoms, C5, C10, C15, and C20, from the least-squares plane of the $[Fe(C_{20}N_4)]$ core are −0.675(9), +0.623(8), −0.579(8), and +0.640(8) Å, respectively. We also report the spectroscopic results of $[Fe(OEP)(^tBuNC)_2]^+$ and $[Fe(ProtoIXMe_2)(^tBuNC)_2]^+$. The porphyrins of these complexes have a_{1u} HOMO, while those of the other complexes examined in this study have a_{2u} HOMO.[36] On the basis of the spectroscopic results, we have concluded that the low-spin complexes with highly saddled porphyrin ring or with a_{1u} porphyrin HOMO resist to switch the ground-state electron configuration from $(d_{xy})^2(d_{xz}, d_{yz})^3$ to $(d_{xz}, d_{yz})^4(d_{xy})^1$.

Scheme 1

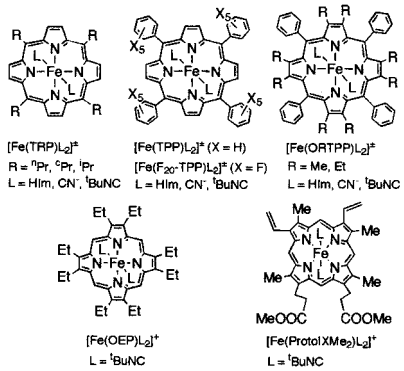

Experimental Section

Spectral Measurement. ^{1}H and ^{13}C NMR spectra were recorded on a JEOL LA300 spectrometer operating at 300.4 MHz for ^{1}H. Chemical shifts were referenced to the residual peak of dichloromethane (δ = 5.32 ppm for ^{1}H and 53.8 ppm for ^{13}C). Proton homonuclear COSY spectra were collected after the measurement of the standard 1D reference spectra. The 2D COSY spectra were collected by use of 1024 points in t_2 over the bandwidth of 8.4 kHz with 512 t_1 blocks and 128 scans per block in which 4 dummy scans were included. UV−vis spectra were recorded on a Hitachi 200-10 spectrophotometer at 25 °C

Py: pyridine. $[Fe(ORTPP)(CN)_2]^-$: (dicyano)[(2,3,7,8,12,13,17,18-octaalkyl-5,10,15,20-tetraphenylporphyrinato)iron(III)] anion. $[Fe(ORTPP)(^tBuNC)_2]^+$: bis(*tert*-butylisocyanide)[(2,3,7,8,12,13,17,18-octaalkyl-5,10,15,20-tetraphenylporphyrinato)iron(III)] cation.

(11) Nakamura, M.; Nakamura, N. *Chem. Lett.* **1991**, 1885−1888.
(12) Nakamura, M.; Ikeue, T.; Neya, S.; Funasaki, N.; Nakamura, N. *Inorg. Chem.* **1996**, *35*, 3731−3732.
(13) Nakamura, M.; Ikeue, T.; Fujii, H.; Yoshimura, T. *J. Am. Chem. Soc.* **1997**, *119*, 6284−6291.
(14) Nakamura, M.; Ikeue, T.; Fujii, H.; Yoshimura, T.; Tajima, K. *Inorg. Chem.* **1998**, *37*, 2405−2414.
(15) Wojaczynski, J.; Latos-Grazynski, L.; Glowiak, T. *Inorg. Chem.* **1997**, *36*, 6299−6306.
(16) Wolowiec, S.; Latos-Grazynski, L.; Mazzanti, M.; Marchon, J.-C. *Inorg. Chem.* **1997**, *36*, 5761−5771.
(17) Wolowiec, S.; Latos-Grazynski, L.; Toronto, D.; Marchon, J.-C. *Inorg. Chem.* **1998**, *37*, 724−732.
(18) Ikeue, T.; Ohgo, Y.; Saitoh, T.; Nakamura, M.; Fujii, H.; Yokoyama, M. *J. Am. Chem. Soc.* **2000**, *122*, 4068−4076.
(19) Senge, M. O.; Medforth, C. J.; Forsyth, T. P.; Lee, D. A.; Olmstead, M. M.; Jentzen, W.; Pandey, R. K.; Shelnutt, J. A.; Smith, K. M. *Inorg. Chem.* **1997**, *36*, 1149−1163.
(20) Jentzen, W.; Simpson, M. C.; Hobbs, J. D.; Song, X.; Ema, T.; Nelson, N. Y.; Medforth, C. J.; Smith, K. M.; Veyrat, M.; Mazzanti, M.; Ramasseul, R.; Marchon, J.-C.; Takeuchi, T.; Goddard, III, W. A.; Shelnutt, J. A. *J. Am. Chem. Soc.* **1995**, *117*, 11085−11097.
(21) Shelnutt, J. A.; Song, X.-Z.; Ma, J.-G.; Jia, S.-L.; Jentzen, W.; Medforth, C. J. *J. Chem. Soc. Rev.* **1998**, *27*, 31−41.
(22) Ma, J.-G.; Zhang, J.; Franco, R.; Jia, S.-L.; Moura, I.; Moura, J. G.; Kroneck, P. M. H.; Shelnutt, J. A. *Biochemistry* **1998**, *37*, 12431−12442.
(23) Bushnell, G. W.; Louie, G. V.; Brayer, G. D. *J. Mol. Biol.* **1990**, *214*, 585−595.
(24) Kunishima, N.; Fukuyama, K.; Matsubara, H.; Htanaka, H.; Shibano, Y.; Amachi, T. *J. Mol. Biol.* **1994**, *235*, 331−344.
(25) Barkigia, K. M.; Berber, M. D.; Fajer, J.; Medforth, C. J.; Renner, M. W.; Smith, K. M. *J. Am. Chem. Soc.* **1990**, *112*, 8851−8857.
(26) Sparks, L. D.; Medforth, C. J.; Park, M.-S.; Chamberlain, J. R.; Ondrias, M. R.; Senge, M. O.; Smith, K. M.; Shelnutt, J. A. *J. Am. Chem. Soc.* **1993**, *115*, 581−592.
(27) Renner, M. W.; Barkigia, K. M.; Zhang, Y.; Medforth, C. J.; Smith, K. M.; Fajer, J. *J. Am. Chem. Soc.* **1994**, *116*, 8582−8592.
(28) Cheng, R.-J.; Chen, P.-Y.; Gau, P.-R.; Chen, C.-C.; Peng, S.-M. *J. Am. Chem. Soc.* **1997**, *119*, 2563−2569.
(29) Ema, T., Senge, M. O., Nelson, N. Y., Ogoshi, H., Smith K. M. *Angew. Chem., Int. Ed. Engl.* **1994**, *33*, 1879−1881.
(30) Ikeue, T.; Ohgo, Y.; Uchida, A.; Nakamura, M.; Fujii, H.; Yokoyama, M. *Inorg. Chem.* **1999**, *38*, 1276−1281.
(31) Mazzanti, M.; Marchon, J.-C.; Wojaczynski, J.; Wolowiec, S.; Latos-Grazynski, L.; Shang, M.; Scheidt, W. R. *Inorg. Chem.* **1998**, *37*, 2476−2481.
(32) Veyrat, M.; Ramasseul, R.; Turowska-Tyrk, I.; Scheidt, W. R.; Autret, M.; Kadish, K. M.; Marchon, J.-C. *Inorg. Chem.* **1999**, *38*, 1772−1779.
(33) Ohgo, Y.; Ikeue, T.; Nakamura, M. *Acta Crystallogr.* **1999**, *C55*, 1817−1818.
(34) Ohgo, Y.; Saitoh, T.; Nakamura, M. *Acta Crystallogr.* **1999**, *C55*, 1284−1286.
(35) Ohgo, Y.; Saitoh, T.; Nakamura, M. *Acta Crystallogr.* **2001**, *C57*, 233−234.
(36) Fajer, J.; Davis, M. S. Electron Spin Resonance of Porphyrin π Cations and Anions. In *The Porphyrins*; Dolphin, D., Ed. Academic Press: New York, 1979; Vol. IV, pp 198−256.

using CH_2Cl_2 as solvent. EPR spectra were measured at 4.2 K with a Brucker ESP-300E spectrometer operating at X band and equipped with an Oxford helium cryostat. The samples for the EPR measurement were prepared by the addition of 4 to 6 equiv of the ligands into the CH_2Cl_2 solutions of [Fe(Porphyrin)Cl] or [Fe(Porphyrin)]ClO_4. The concentrations of EPR samples were 5∼8 mM. The observed EPR spectra had enough quality to determine their *g* values from the spectra except for some broad signals. In the latter case, the *g*-values were estimated by the simulation of the observed spectra using Bruker WIN-EPR Sim Fonia program.

Synthesis. Free base porphyrins. H_2(TRP)(R = ^{n}Pr,[37] ^{c}Pr,[18] and ^{i}Pr[29,38]), H_2(TPP), H_2(OMTPP),[25] and H_2(OETPP),[25] were prepared from the corresponding aldehydes and pyrroles according to the literature. H_2(OEP) and H_2(ProtoIXMe$_2$) were purchased from Aldrich. The *meso* ^{13}C enriched H_2(TPP), H_2(OMTPP), and H_2(OETPP) were prepared similarly with the use of benzaldehyde-carbonyl-^{13}C (99 atom % ^{13}C) purchased from Aldrich.

[Fe(Porphyrin)Cl](Porphyrin = TRP, TPP, F_{20}-TPP, ORTPP, OEP, ProtoIXMe$_2$). Insertion of iron was performed using $FeCl_2 \cdot 4H_2O$ either in refluxing $CH_3OH-CHCl_3$ (1:3) for H_2(TRP), H_2(OEP), and H_2(ProtoIXMe$_2$) or in refluxing DMF for H_2(ORTPP).[18,28] The Fe(III) porphyrin complexes thus formed were treated with diluted HCl and purified by chromatography on silica gel using $CH_2Cl_2-CH_3OH$ as eluents. Formation of [Fe(TRP)Cl], [Fe(ORTPP)Cl], [Fe(OEP)Cl], and [Fe(ProtoIXMe$_2$)Cl] was confirmed by the comparison with the UV−vis and ^{1}H NMR spectral properties reported before.[13,18,28,30] [Fe(F_{20}-TPP)Cl] was purchased from Aldrich.

[Fe(Porphyrin)(THF)$_2$]ClO_4(Porphyrin = TRP, TPP, F_{20}-TPP, ORTPP, OEP, ProtoIXMe$_2$). A THF solution (5 mL) of $AgClO_4$ (3.5×10^{-5} mol) was added to a THF solution (20 mL) of [Fe(Por)Cl] (3.5×10^{-5} mol). The solution was stirred for a minute at room temperature and then evaporated. *Caution! Perchlorate salts are potentially explosive when heated or shocked. Handle them in milligram quantities with care.* Dichloromethane (20 mL) was added to the reaction mixture and the resultant suspension was filtered to remove silver chloride. After the evaporation of the filtrate, 20 mL of THF was added to dissolve the solid and then 20 mL of heptane was added. The solution was allowed to stand overnight. The purple crystal thus formed was collected by filtration, washed with hexane, and dried in vacuo for 10 min at 25 °C.[39]

[Fe(T^{i}PrP)(THF)$_2$]ClO_4. Yield: 69%. ^{1}H NMR (CD_2Cl_2, 25 °C, δ): −34.8(8H, Py-H), 13.0(4H, *meso* α-H), 5.0(24H, *meso* β-H), 4.5(8H, THF), 9.5(8H, THF). EPR(CH_2Cl_2, 4.2 K): $g = 3.99, 1.97$. Mössbauer (microcrystalline, 76 K): IS = 0.34 mm s^{-1}, QS = 3.71 mm s^{-1}. SQUID (microcrystalline, μ_{eff}): $3.90 \pm 0.10\ \mu_B$ in 50 ∼ 300 K.[40] The crystal structure of this complex was reported elswhere.[35]

[Fe(T^{c}PrP)(THF)$_2$]ClO_4. Yield: 70%. ^{1}H NMR (CD_2Cl_2, 25 °C, δ): −35.3(8H, Py-H), 32.8(4H, *meso* α-H), 0.89(8H, *meso* β-H), 2.79(8H, *meso* β-H), 7.6(8H, THF), 12.5(8H, THF).

[Fe(T^{n}PrP)(THF)$_2$]ClO_4. Yield: 77%. ^{1}H NMR (CD_2Cl_2, 25 °C, δ): −19.0(8H, Py-H), 15.6(8H, *meso* α-H), 4.97(8H, *meso* β-H), 2.86(12H, *meso* γ-H), 9.5(8H, THF), 14.6(8H, THF).

[Fe(F_{20}-TPP)(THF)$_2$]ClO_4. Yield: 65%. ^{1}H NMR (CD_2Cl_2, 25 °C, δ): 41.4(8H, Py-H), 7.9(8H, THF), 19.4(8H, THF).

[Fe(OMTPP)(THF)$_2$]ClO_4. Yield: 67%. ^{1}H NMR (CD_2Cl_2, −20 °C, δ): 71.5(24H, CH_3), 13.8(8H, *o*), 6.88(8H, *m*), 10.40(4H, *p*), 9.4(8H, THF), 13.8(8H, THF). Another signal for the coordinated THF ligand might be too broad to detect.

[Fe(OETPP)(THF)$_2$]ClO_4. Yield: 87%. ^{1}H NMR (CD_2Cl_2, 25 °C, δ): 42.7(8H, CH_2), 14.2(8H, CH_2), 0.67(24H, CH_3), 12.9(8H, *o*), 6.5(8H, *m*), 10.6(4H, *p*), 11.4(8H, THF). EPR(CH_2Cl_2, 4.2 K): $g =$ 4.01, 2.00. Mössbauer (microcrystalline, 80 K): IS = 0.50 mm s^{-1}, QS = 3.50 mm s^{-1}. SQUID (microcrystalline, μ_{eff}): $3.85 \pm 0.05\ \mu_B$ in 20∼300 K.[40]

[Fe(OEP)(THF)$_2$]ClO_4.[41] ^{1}H NMR (CD_2Cl_2, 25 °C, δ): 10.3(4H, *meso*), 34.6(16H, CH_2), 6.2(24H, CH_3). Coordinated THF ligand showed very broad signals at 10.3 and 6.0 ppm.

[Fe(ProtoIXMe$_2$)(THF)$_2$]ClO_4. ^{1}H NMR (CD_2Cl_2, 25 °C, δ): 69.3(3H, CH_3), 68.4(3H, CH_3), 66.6(3H, CH_3), 62.5(3H, CH_3), 50.5(1H, vinyl-α), 48.3(1H, vinyl-α), 40.0(2H, α-CH_2), 39.5(2H, α-CH_2), 6.7(4H, β-CH_2 x 2), 3.64(6H, OCH_3 x 2), −8.99(1H, vinyl-β), −9.17(1H, vinyl-β), −10.39(1H, vinyl-β), −10.59(1H, vinyl-β). Broad signals were observed at 22 and 11 ppm due to the coordinated THF.

[Fe(Porohyrin)(HIm)$_2$]Cl (Porphyrin = TRP, TPP). These complexes were prepared by the addition of 4 to 6 equiv of imidazole into a CD_2Cl_2 solution of [Fe(Porphyrin)Cl] placed in an NMR sample tube as described in our previous paper.[18]

[Fe(F_{20}-TPP)(1-MeIm)$_2$]Cl. This complex was prepared by the addition of 4 equiv of 1-methylimidazole into a CD_2Cl_2 solution of [Fe(F_{20}-TPP)Cl] placed in an NMR sample.^{1}H NMR (CD_2Cl_2, 25 °C, δ): −15.9(8H, Py-H), 19.4(6H, CH_3), −7.18(2H, ligand).

[Fe(ORTPP)(HIm)$_2$]ClO_4 (R = Me, Et). A large excess of HIm was necessary for the complete conversion of [Fe(ORTPP)Cl] into [Fe(ORTPP)(HIm)$_2$]Cl. Thus, [Fe(ORTPP)−(THF)$_2$]ClO_4 was used instead of [Fe(ORTPP)Cl]. The CD_2Cl_2 solution of [Fe(ORTPP)−(THF)$_2$]ClO_4 was treated with 4 to 6 equiv of HIm in an NMR sample tube. Formation of [Fe(ORTPP)(HIm)$_2$]ClO_4 was confirmed by the ^{1}H and ^{13}C NMR spectra at 25 °C.

[Fe(OMTPP)(HIm)$_2$]ClO_4. ^{1}H NMR (CD_2Cl_2, 25 °C, δ): 21.1(24H, CH_3), 5.42(8H, *o*), 6.21(8H, *m*), 6.79(4H, *p*). The ligand exchange was fast on the ^{1}H NMR time scale at 25 °C. As a result, the free and the coordinated ligands gave broad signals at the average positions. The ligand exchange became slow below −40 °C to show the coordinated ligand signals separately. ^{1}H NMR (CD_2Cl_2, −79 °C, δ): 23.0(24H, CH_3), 1.79(8H, *o*), 4.39(8H, *m*), 5.40(4H, *p*), 20.6(2H, ligand), 13.0(2H, ligand), −4.6(2H, ligand). ^{13}C NMR (CD_2Cl_2, 25 °C, δ): 128.4(s, α-Py), 173.0(s, β-Py), −33.4(q, CH_3), 28.5(s, *meso*), 153.4(s, *ipso*), 116.6(d, *o*), 126.4(d, *m*), 125.9(d, *p*).

[Fe(OETPP)(HIm)$_2$]ClO_4. ^{1}H NMR (CD_2Cl_2, 25 °C, δ): 4.5(broad, 8H, CH_2), ca. 10 (broad, 8H, CH_2), 0.86(24H, CH_3), 4.96(8H, *o*), 5.79(8H, *m*), 6.72(4H, *p*). The ligand exchange was fast on the ^{1}H NMR time scale at 25 °C. However, the process was frozen below −20 °C, giving the signals of the coordinated HIm ligand. ^{1}H NMR (CD_2Cl_2, −70 °C, δ): 2.84(8H, CH_2), 12.50(8H, CH_2), 1.41(24H, CH_3), 2.09(8H, *o*), 4.31(8H, *m*), 5.76(4H, *p*), 22.2(2H, ligand), 17.5(2H, ligand), 14.6(2H, ligand). ^{13}C NMR (CD_2Cl_2, 25 °C, δ): 162.4(s, α-Py), 167.0(s, β-Py), −23.5(t, CH_2), 86.6(q, CH_3), 7.0(s, *meso*), 164.0(s, *ipso*); 107.4(d, *o*); 124.6(d, *m*); 125.0(d, *p*).

[Fe(Porphyrin)(CN)$_2$]NBu_4 (Porphyrin = TRP, TPP, F_{20}-TPP, ORTPP). These complexes were prepared by the addition of 4 to 6 equiv of tetrabutylammonium cyanide into a CD_2Cl_2 solution of [Fe(Porphyrin)Cl] placed in an NMR sample tube as described in our previous papers.[13,18] Formation and spectroscopic results of [Fe(TRP)(CN)$_2$]NBu_4(R = ^{i}Pr, ^{c}Pr, ^{n}Pr) and [Fe(TPP)(CN)$_2$]NBu_4 have already been reported.[13,18, 42,43]

[Fe(F_{20}-TPP)(CN)$_2$]NBu_4. ^{1}H NMR (CD_2Cl_2, 25 °C, δ): −19.4(8H, Py-H). ^{13}C NMR (CD_2Cl_2, 25 °C, δ): 48.6(s, α-Py), 92.0(d, β-Py), 32.9(s, *meso*), 109.4(t, $^2J_{C-F}$ = 18.1 Hz, *ipso*), 142.8(d, $^1J_{C-F}$ = 244 Hz, *o*), 134.8(d, $^1J_{C-F}$ = 256 Hz, *m*), 139.7(d, $^1J_{C-F}$ = 256 Hz, *p*).

[Fe(OMTPP)(CN)$_2$]NBu_4. ^{1}H NMR (CD_2Cl_2, 25 °C, δ): 13.36(24H, CH_3), 5.43(8H, *o*), 7.16 (8H, *m*), 6.58(4H, *p*). ^{13}C NMR (CD_2Cl_2, 25 °C, δ): 85.3(s, α-Py), 127.2(s, β-Py), −23.2 (q, CH_3), 136.6(s, *meso*), 123.2(s, *ipso*), 166.8(d, *o*), 131.7(d, *m*), 127.6(d, *p*).

[Fe(OETPP)(CN)$_2$]NBu_4. ^{1}H NMR (CD_2Cl_2, 25 °C, δ): 0.78(24H, CH_3); 6.87(16H, CH_2); 5.39(8H, *o*); 6.48(8H, *m*); 6.56(4H, *p*). ^{13}C NMR

(37) Neya, S.; Funasaki, N. *J. Heterocycl. Chem*. **1997**, *34*, 689−690.
(38) Wagner, R. W.; Lawrence, D. S.; Lindsey, J. S. *Tetrahedron Lett*. **1987**, *28*, 3069−3070.
(39) Full report on the formation, characterization, and spectroscopic properties of [Fe(Porphyrin) (THF)$_2$]ClO_4 will be published elsewhere. [Fe(T^{i}PrP)(THF)$_2$]ClO_4 and [Fe(OETPP)(THF$_2$)]ClO_4 turned out to be very pure intermediate spin ($S = {}^3/_2$) complexes.[40]
(40) Ikeue, T.; Saitoh, T.; Yamaguchi, T.; Ohgo, Y.; Nakamura, M.; Takahashi, M.; Takeda, M. *Chem. Commun*. **2000**, 1989−1990.
(41) Ogoshi, H.; Sugimoto, H.; Watanabe, E.; Yoshida, Z.; Maeda, Y.; Sakai, H.; *Bull. Chem. Soc. Jpn*. **1981**, *54*, 3414−3419.
(42) La Mar, G. N.; Gaudio, J. D.; Frye, J. S. *Biochim. Biophys. Acta* **1977**, *498*, 422−435.
(43) Nakamura, M.; Ikeue, T.; Ikezaki, A.; Ohgo, Y.; Fujii, H. *Inorg. Chem*. **1999**, *38*, 3857−3862.

(CD_2Cl_2, 25 °C, δ): 134.9(s, α-Py), 140.6(s, β-Py), −19.9(t, CH_2), 74.6 (q, CH_3), 71.7(s, *meso*), 145.6(s, *ipso*), 136.4(d, *o*), 126.5(d, *m*), 125.9(d, *p*).

[Fe(Porphyrin)(^{t}BuNC)$_2$]ClO$_4$ (Porphyrin = TRP, TPP, F$_{20}$-TPP, ORTPP, OEP, ProtoIXMe$_2$). Complete formation of [Fe(Porphyrin)(^{t}BuNC)$_2$]Cl was unsuccessful even by the addition of large excess ^{t}BuNC into a CD_2Cl_2 solution of [Fe(Porphyrin)Cl]. Thus, [Fe(Porphyrin)(THF)$_2$]ClO_4 was used instead of [Fe(Porphyrin)Cl]. The CD_2Cl_2 solution of [Fe(Porphyrin)(THF)$_2$]ClO_4 was treated with 4 to 6 equiv of ^{t}BuNC in an NMR sample tube. Formation of [Fe(Porphyrin)(^{t}BuNC) $_2$]ClO_4 was confirmed at 25 °C by the ^{1}H and ^{13}C NMR spectra.

[Fe(T^{i}PrP)(^{t}BuNC)$_2$]ClO$_4$. ^{1}H NMR (CD_2Cl_2, 25 °C, δ): 11.97(8H, Py-H), 39.51 (8H, CH), 8.05(24H, CH_3), −1.74(18H, CH_3 of the coordinated ^{t}BuNC). ^{13}C NMR (CD_2Cl_2, 25 °C, δ): 98.8(d, β-Py), 18.0(q, CH_3 of the coordinated ^{t}BuNC).

[Fe(T^{c}PrP)(^{t}BuNC)$_2$]ClO$_4$. ^{1}H NMR (CD_2Cl_2, 25 °C, δ): 13.12(8H, Py-H), −2.21(8H, CH_2), −3.16(8H, CH_2), −2.04(18H, CH_3 of the coordinated ^{t}BuNC). The *meso* CH signal was not observed up to δ 500 ppm. ^{13}C NMR (CD_2Cl_2, 25 °C, δ): 91.0(d, β-Py), 16.4(q, CH_3 of the coordinated ^{t}BuNC).

[Fe(T^{n}PrP)(^{t}BuNC)$_2$]ClO$_4$. ^{1}H NMR (CD_2Cl_2, 25 °C, δ): 11.60(8H, Py-H), 95.20(8H, α-CH_2), −2.15(8H, β-CH_2), 2.17(12H, γ-CH_3), −1.53(18H, CH_3 of the coordinated ^{t}BuNC). ^{13}C NMR (CD_2Cl_2, 25 °C, δ): 84.7 (d, β-Py), 29.5 (q, γ-CH_3), 18.4(q, CH_3 of the coordinated ^{t}BuNC).

[Fe(TPP)(^{t}BuNC)$_2$]ClO$_4$. ^{1}H NMR (CD_2Cl_2, 25 °C, δ): 0.77(8H, *o*), 14.09(8H, *m*), 3.12(4H, *p*), 10.01(8H, Py-H), −1.86(18H, CH_3 of the coordinated ^{t}BuNC). ^{13}C NMR (CD_2Cl_2, 25 °C, δ): −293.6(s, α-Py), 82.8(d, β-Py), −122.5(s, *ipso*), 457.6(broad-s, *o*), 145.8(d, *m*), 154.4(d, *p*), 767.0(s, *meso*), 19.3(q, CH_3 of the coordinated ^{t}BuNC). The *meso* carbon signal was observable only when the *meso*-^{13}C enriched complex was used.

[Fe(F$_{20}$-TPP)(^{t}BuNC)$_2$]ClO$_4$. ^{1}H NMR (CD_2Cl_2, 25 °C, δ): 4.31(8H, Py-H), −1.86(18H, CH_3 of the coordinated ^{t}BuNC).

[Fe(OMTPP)(^{t}BuNC)$_2$]ClO$_4$. ^{1}H NMR (CD_2Cl_2, 25 °C, δ): 1.26(24H, CH_3); 3.06(8H, o); 12.83(8H, m); 5.16(4H, p). The *tert*-butyl protons of the coordinated ligand gave a broad signal due to the exchange with the free ligand at 25 °C. The broad signal split into two signals below 0 °C, where the coordinated ligand gave a signal corresponding to 18H. ^{1}H NMR (CD_2Cl_2, −20 °C, δ): −0.49(24H, CH_3), 1.96(8H, o), 13.95(8H, m), 4.70(4H, p), −2.24 (18H, CH_3 of the coordinated ^{t}BuNC). ^{13}C NMR (CD_2Cl_2, 25 °C, δ): −205.3(s, α-Py), 112.9(s, β-Py), 12.4 (q, CH_3), 701.4(s, *meso*), −84.4(s, *ipso*), 430.2(broad s, *o*), 155.8(d, *m*), 142.6(d, *p*). The *meso* carbon signal was observable only when the *meso*-^{13}C enriched complex was used. The *tert*-butyl carbons of the coordinated ligand gave a broad signal at 25.9 ppm due to the fast exchange with the free ligand at 25 °C. The broad signal split into two sets of quartets below −20 °C, where coordinated ligand showed signals at δ 13.7 ppm.

[Fe(OETPP)(^{t}BuNC)$_2$]ClO$_4$. ^{1}H NMR (CD_2Cl_2, 25 °C, δ): 7.46(16H, CH_2), 1.08(24H, CH_3), 5.54(8H, o), 11.05(8H, m), 6.31(4H, p). The *tert*-butyl protons of the coordinated ligand showed a broad signal at 25 °C, which split into two below 0 °C. At −20 °C, the coordinated ^{t}BuNC gave a signal at −2.10 ppm with integral intensity of 18H. ^{1}H NMR (CD_2Cl_2, −20 °C, δ): 8.35(16H, CH_2), 1.41(24H, CH_3), 5.57(8H, o), 11.42(8H, m), 6.30(4H, p), −2.10(18H, CH_3 of the coordinated ^{t}-BuNC). ^{13}C NMR (CD_2Cl_2, 25 °C, δ): −3.7(s, α-Py), 144.2(s, β-Py), −0.5(t, CH_2), 59.1(q, CH_3), 417.5(s, *meso*), 38.0(s, *ipso*), 309.6(d, *o*), 145.2(d, *m*), 138.6(d, *p*). Although the methyl carbons of the coordinated ligand did not show the separate signal due to the fast ligand exchange at 25 °C, a new quartet assigned to these carbons appeared at 22.9 ppm at −50 °C.

[Fe(OEP)(^{t}BuNC)$_2$]ClO$_4$. ^{1}H NMR (CD_2Cl_2, 25 °C, δ): 7.61(16H, CH_2), 3.19(24H, CH_3), −37.7(4H, *meso*), −0.81(18H, CH_3 of the coordinated ^{t}BuNC). ^{13}C NMR (CD_2Cl_2, 25 °C, δ): −94.9(s, α-Py), 115.9(s, β-Py), 1.7(t, CH_2), 59.1(q, CH_3), 371.4 (s, *meso*), 25.7(q, CH_3 of the coordinated ^{t}BuNC).

[Fe(ProtoIXMe$_2$)(^{t}BuNC)$_2$]ClO$_4$. ^{1}H NMR (CD_2Cl_2, 25 °C, δ): 12.41(1H, α-vinyl), 11.91 (1H, α-vinyl), 11.44(3H, CH_3), 11.21(3H, CH_3), 11.18(3H, CH_3), 10.76(3H, CH_3), 7.19(4H, α-CH_2 × 2), 4.03(4H, β-CH_2 × 2), 4.90(1H, β-vinyl), 4.66(1H, β-vinyl), 4.27(1H, β-vinyl), 4.07(1H, β-vinyl), 3.75(6H, OCH_3 × 2), −45.04(1H, *meso*), −44.67(1H, *meso*), −43.98(1H, *meso*), −1.33 (18H, CH_3 of the coordinated ^{t}BuNC). ^{13}C NMR (CD_2Cl_2, 25 °C, δ): −101(broad s, α-Py), −113(broad s, α-Py), 396 (broad s, *meso*), 26.8 (q, CH_3 of the coordinated ^{t}BuNC).

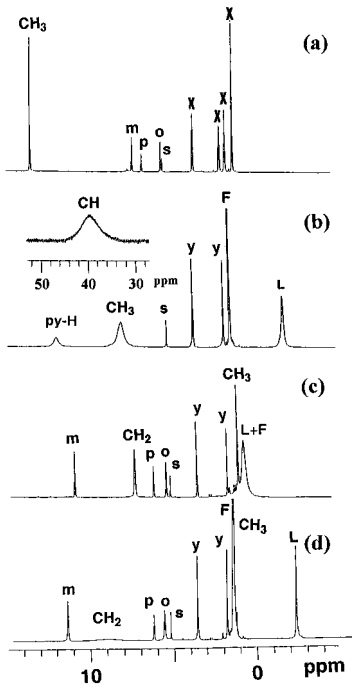

Figure 1. ^{1}H NMR spectra of (a) [Fe(OMTPP)(CN)$_2$]$^-$, (b) [Fe(T^{i}PrP)(^{t}BuNC)$_2$]$^+$, and (c) [Fe(OETPP)(^{t}BuNC)$_2$]$^+$ taken in CD_2Cl_2 at 25 °C. (d) ^{1}H NMR of [Fe(OETPP)(^{t}BuNC)$_2$]$^+$ taken in CD_2Cl_2 at −40 °C. Integral intensity of the methyl signal of the coordinated ^{t}BuNC ligand, δ −2.50 ppm, clearly shows the formation of the bis-adduct. Signal assignment: o, m, and p, *ortho*-H, *meta*-H, and *para*-H; CH_3, pyrrole-methyl; CH_2, pyrrole-methylene; L and F, methyl signal of the coordinated and free ^{t}BuNC ligand, respectively; x, tetrabutylammonium ion; y, THF; s, dichloromethane.

Results

^{1}H NMR Spectra. Table 1 shows the ^{1}H NMR chemical shifts of [Fe(TRP)L$_2$]$^\pm$, [Fe(TPP)L$_2$]$^\pm$, [Fe(F$_{20}$-TPP)L$_2$]$^\pm$, and [Fe(ORTPP)L$_2$]$^\pm$ (L = HIm, CN$^-$, and ^{t}BuNC) taken at −50 °C in CD_2Cl_2 solution together with the labeling of the proton atoms. The chemical shifts of [Fe(OEP)(^{t}BuNC)$_2$]$^+$ and [Fe(ProtoIXMe$_2$)(^{t}BuNC)$_2$]$^+$ are also listed. Signal assignments of these complexes were unambiguously done by the integral intensities, coupling patterns, and 2D COSY technique. Figures 1a, 1b, and 1c show the ^{1}H NMR spectra of [Fe(OMTPP)(CN)$_2$]$^-$, [Fe(T^{i}PrP)(^{t}BuNC)$_2$]$^+$, and [Fe(OETPP)(^{t}BuNC)$_2$]$^+$, respectively, taken at 25 °C as typical examples. In contrast to the case of [Fe(T^{i}PrP)(^{t}BuNC)$_2$]$^+$ shown in Figure 1b, the ligand exchange process is fast on the ^{1}H NMR time scale in [Fe(OETPP)(^{t}BuNC)$_2$]$^+$; a broad signal corresponding to the methyl protons of the free and coordinated ligands appeared at ca. 1 ppm. Figure 1d shows the ^{1}H NMR spectrum of [Fe(OETPP)(^{t}BuNC)$_2$]$^+$ taken at −40 °C. The ligand exchange process is frozen at this temperature; the *tert*-butyl signal of the coordinated ^{t}BuNC is observed at −2.5 ppm with the integral intensity of 18 H. The methylene signal appears at 9.2 ppm as a very broad singlet due to the ring inversion. This signal split into two peaks below −60 °C and gave clearly separated signals at 5.68 and 18.40 ppm at −80 °C where the ring inversion process is frozen on the ^{1}H NMR time scale. The chemical shifts of the pyrrole-H and pyrrole-CH(α) signals of these complexes are plotted against

Table 1. ^{1}H NMR Chemical Shifts of [Fe(Porphyrin)L_2]$^{\pm}$ Taken in CD_2Cl_2 Solution at −50 °C

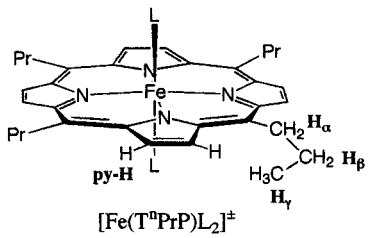

[Fe(T^{n}PrP)L_2]$^{\pm}$

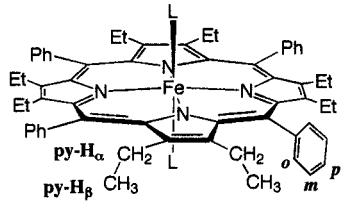

[Fe(OETPP)L_2]$^{\pm}$

		pyrrole			*meso*				aryl				
porphyrins	L	py-H	py-H$_\alpha$	py-H$_\beta$	*meso*	H$_\alpha$	H$_\beta$	H$_\gamma$	o	m	p	^{t}Bu	ref
T^{i}PrP	HIm	0.11	−	−	−	16.14	3.91	−	−	−	−	−	18
T^{c}PrP	HIm	−18.70	−	−	−	10.88	−1.52	−	−	−	−	−	18
							−2.26						
T^{n}PrP	HIm	−21.45	−	−	−	1.72	−1.47	−0.46	−	−	−	−	18
TPP	HIm	−26.05	−	−	−	−	−	−	3.52	5.44	5.78	−	this work[a]
F$_{20}$-TPP	1-MeIm[b]	−24.42	−	−	−	−	−	−	−	−	−	−	this work
OMTPP	HIm	−	20.89	−	−	−	−	−	2.91	5.03	5.84	−	this work
OETPP	HIm	−	3.21	1.28	−	−	−	−	2.76	4.68	5.99	−	this work
			11.81										
T^{i}PrP	CN$^-$	12.26	−	−	−	28.68	6.67	−	−	−	−	−	18
T^{c}PrP	CN$^-$	4.28	−	−	−	91.87	−0.15	−	−	−	−	−	18
							−1.83						
T^{n}PrP	CN$^-$	−3.48		−	−	30.91	0.09	0.82	−	−	−	−	18
TPP	CN$^-$	−28.73	−	−	−	−	−	−	2.12	4.93	4.96	−	this work[c]
F$_{20}$-TPP	CN$^-$	−32.51	−	−	−	−	−	−	−	−	−	−	this work
OMTPP	CN$^-$	−	18.35	−	−	−	−	−	3.56	6.12	5.84	−	this work
OETPP	CN$^-$	−	7.89	0.81	−	−	−	−	3.90	6.54	6.30	−	this work
T^{i}PrP	^{t}BuNC	12.93	−	−	−	50.80	10.03	−	−	−	−	−2.36	this work
T^{c}PrP	^{t}BuNC	14.70	−	−	−	*d*	−4.23	−	−	−	−	−2.73	this work
T^{n}PrP	^{t}BuNC	12.65	−	−	−	118.50[e]	−4.16	2.28	−	−	−	−2.12	this work
TPP	^{t}BuN[c]	11.72	−	−	−	−	−	−	−2.38	16.50	0.88	−2.86	this work[f]
F$_{20}$-TPP	^{t}BuNC	5.48	−	−	−	−	−	−	−	−	−	−3.03	this work
OMTPP	^{t}BuNC	−	−2.13	−	−	−	−	−	0.99	14.99	4.24	−2.70	this work
OETPP	^{t}BuN[c]	−	9.77[g]	1.36	−	−	−	−	5.84	11.54	6.43	−2.84	this work
OEP	^{t}BuNC	−	7.40	3.74	−58.2	−	−	−	−	−	−	−1.32	this work[h]
ProtolXMe$_2$	^{t}BuNC	−	*i*	*i*	−70.4	−	−	−	−	−	−	−2.55	this work
					−71.5								

[a] Reported by Satterlee and La Mar, ref 57. [b] 1-MeIm was used instead of HIm due to the low solubility of the bis(HIm) complex. [c] Originally reported by La Mar et al., ref 42. [d] Signals were not observed up to δ 500 ppm. [e] Extrapolated value. This signal disappeared below −20 °C. [f] Originally reported by Simonneaux et al., ref 2. [g] Extrapolated value. Signals are too broad due to the ring inversion at −50 °C. At −80 °C, two signals appeared at 5.68 and 18.40 ppm. [h] Originally reported by Walker et al., ref 6. [i] Ring CH_3: 9.89, 9.62, 9.58, 9.41. Vinyl(α): 11.42, 10.96. Vinyl(*β*): 6.25, 5.93, 5.39, 5.11. CH_2(α): 6.62. CH_2(*β*): 4.57; OCH3; 3.79.

inverse temperature. They are shown in the Supporting Information.

^{13}C NMR Spectra. Table 2 shows the ^{13}C NMR chemical shifts of [Fe(TRP)L_2]$^{\pm}$, [Fe(TPP)L_2]$^{\pm}$, and [Fe(ORTPP)L_2]$^{\pm}$ (L = HIm, CN$^-$, and ^{t}BuNC) taken at −50 °C in CD_2Cl_2 solution together with the labeling of the carbon atoms. The chemical shifts of [Fe(OEP)(^{t}BuNC)$_2$]$^+$ and [Fe(ProtoIXMe$_2$)(^{t}BuNC)$_2$]$^+$ taken at the same temperature are also listed. Signals were assigned on the basis of the acquisition of the proton-coupled ^{13}C NMR spectra. The *meso* carbon signals in [Fe(ORTPP)L_2]$^{\pm}$ and [Fe(TPP)L_2]$^{\pm}$ were assigned by the use of the *meso*-^{13}C enriched complexes. The α-pyrrole and *ipso*-phenyl carbons of [Fe(ORTPP)(HIm)$_2$]$^+$ and [Fe(ORTPP)(CN)$_2$]$^-$ were conveniently assigned on the basis of their coupling with the adjacent *meso*-carbons in the ^{13}C NMR spectra of the *meso*-^{13}C enriched complexes. In the case of [Fe(TRP)(^{t}BuNC)$_2$]$^+$, only the *β*-pyrrole and the ligand methyl signals were observable; other signals corresponding to the *meso*,*meso*-C$_\alpha$, *meso*-C$_\beta$, and α-pyrrole carbons were too broad to detect. Figures 2a, 2b, and 2c show the proton coupled ^{13}C NMR spectra of [Fe(OETPP)(Him)$_2$]$^+$, [Fe(OMTPP)(CN)$_2$]$^-$, and [Fe(OETPP)(^{t}BuNC)$_2$]$^+$, respectively, taken at 25 °C as typical examples. The proton decoupled ^{13}C NMR spectra of the *meso*-^{13}C enriched complexes are also given in the inset of each figure. Figures 2a and 2b clearly show that both the α-pyrrole and *ipso* carbon signals appear as doublets due to the coupling with the adjacent *meso* carbons. A part of the ^{13}C NMR spectrum of [Fe(OETPP)(^{t}BuNC)$_2$]$^+$ taken at −50 °C is also given in the inset of Figure 2c, which clearly shows the methyl signal of the coordinated ^{t}BuNC ligand at 22.9 ppm.

EPR Spectra. EPR spectra of [Fe(TRP)L_2]$^{\pm}$, [Fe(TPP)L_2]$^{\pm}$, and [Fe(ORTPP)L_2]$^{\pm}$ (L = HIm, CN$^-$, and ^{t}BuNC) were taken at 4.2 K in frozen CH_2Cl_2 solution. Figure 3 shows the observed (bottom) and calculated (top) spectra of [Fe(T^{n}PrP)(^{t}BuNC)$_2$]$^+$, [Fe(OMTPP)(^{t}BuNC)$_2$]$^+$, and [Fe(OETPP)(^{t}BuNC)$_2$]$^+$ as typical examples. In the case of [Fe(TRP)(^{t}BuNC)$_2$], the calculated spectra fitted well to the observed ones with the use of appropriate $g_\perp$ and $g_{||}$ values. The signal fitting was, however, rather poor in the case of [Fe(OMTPP)(^{t}BuNC)$_2$]$^+$ and [Fe(OETPP)(^{t}BuNC)$_2$]$^+$. Since the EPR spectra of these complexes seemed to be rhombic rather than axial, the calculated spectra were obtained with the use of three different *g* values as shown in Figures 3b and 3c. The *g* values of these complexes thus obtained are listed in Table 3 together with those of [Fe(OEP)(^{t}BuNC)$_2$]$^+$ and [Fe(ProtoIXMe$_2$)(^{t}BuNC)$_2$]$^+$ taken at the same temperature.

Table 2. ^{13}C NMR Chemical Shifts of $[Fe(Porphyrin)L_2]^{\pm}$ Taken in CD_2Cl_2 Solution at −50 °C

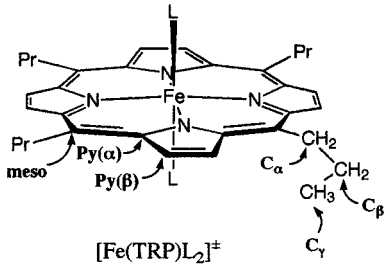

$[Fe(TRP)L_2]^{\pm}$

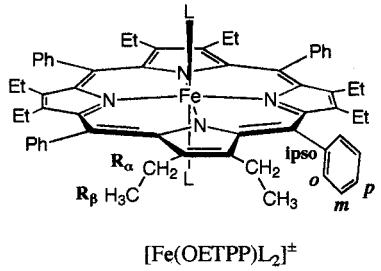

$[Fe(OETPP)L_2]^{\pm}$

		pyrrole				*meso*				aryl			
porphyrins	L	py(α)	py(β)	R_α	R_β	*meso*	C_α(ipso)	C_β	C_γ	o	m	p	ref
T^iPrP	HIm	−28.3	76.5	−	−	331.6	−55.3	172.5	−	−	−	−	18
T^cPrP	HIm	11.8	79.6	−	−	97.1	−6.2	17.5	−	−	−	−	18
T^nPrP	HIm	0.0	73.6	−	−	73.1	14.5	64.5	12.4	−	−	−	18
TPP	HIm	−2.0	77.1	−	−	25.2	(136.9)	−	−	122.9	125.5	123.3	this work
OMTPP	HIm	81.2	145.6	−50.3	−	−11.5	(151.0)	−	−	108.3	122.1	123.9	this work
OETPP	HIm	143.5	156.1	−38.8	104.8	−37.2	(165.8)	−	−	97.1	122.3	122.6	this work
T^iPrP	CN^-	−186.0	54.7	−	−	639.6	−134.5	309.4	−	−	−	−	18
T^cPrP	CN^-	−84.2	61.2	−	−	386.7	−98.9	91.4	−	−	−	−	18
T^nPrP	CN^-	−72.7	61.2	−	−	336.1	−56.6	249.7	17.9	−	−	−	18
TPP	CN−	18.2	86.2	−	−	65.1	(122.9)	−	−	148.0	122.5	125.0	this work[a]
OMTPP	CN^-	81.2	131.6	−43.0	−	87.4	(127.6)	−	−	151.8	128.9	125.4	this work
OETPP	CN^-	128.8	142.4	−34.3	95.7	45.1	(147.1)	−	−	132.5	125.7	125.1	this work
T^iPrP[b]	^{t}BuNC	*c*	98.8	−	−	*c*	*c*	*c*	−	−	−	−	this work
T^cPrP[b]	^{t}BuNC	*c*	91.0	−	−	*c*	*c*	*c*	−	−	−	−	this work
T^nPrP[b]	^{t}BuNC	*c*	84.7	−	−	*c*	*c*	*c*	29.5	−	−	−	this work
TPP	^{t}BuNC	−429.3	60.0	−	−	997.3[d]	(−223.6)	−	−	579.6	149.3	166.5	this work
OMTPP	^{t}BuNC	−376.5[d]	90.2	18.9	−	979.4[d]	(−189.8)	−	−	568.8	169.9	146.3	this work
OETPP	^{t}BuNC	13.3	136.4	−11.0	77.7	416.2	(48.0)	−	−	323.7	146.4	137.4	this work
OEP	^{t}BuNC	−187.4	96.4	1.7	58.6	491.1	−	−	−	−	−	−	this work
ProtoIXMe$_2$	^{t}BuNC	−100.9[b] −117.8[b]	*e*	*e*	*e*	396[b]	−	−	−	−	−	−	this work

[a] Originally reported by Wüthrich and Baumann, ref 47. [b] Data at 25 °C. [c] Signals are too broad to detect. [d] Extrapolated from high temperature. [e] Assignment is not clear.

Table 3. EPR *g* Values of $[Fe(Porphyrin)L_2]^{\pm}$ Taken in Frozen CH_2Cl_2 Solution at 4.2 K Together with the Ground State Electron Configuration

porphyrins	L	g_1	g_2	g_3	ground state[a]	ref
T^iPrP	HIm	2.55	2.55	−	d_{xy}	18
T^cPrP	HIm	2.87	2.42	−	d_π	18
T^nPrP	HIm	2.90	2.35	(1.45)	d_π	18
TPP	HIm	2.87	2.29	1.56	d_π	56
OMTPP	HIm	2.84	2.31	1.58	d_π	this work
OETPP	HIm	2.72	2.37	1.64	d_π	this work
T^iPrP	CN^-	2.42	2.42	1.74	d_{xy}	18
T^cPrP	CN^-	2.47	2.47	−	d_{xy}	18
T^nPrP	CN^-	2.49	2.49	−	d_{xy}	18
TPP	CN^-	3.70	−	−	d_π	73
OMTPP	CN^-	3.48	−	−	d_π	this work
OETPP	CN^-	3.31	−	−	d_π	this work
T^iPrP	^{t}BuNC	2.16	2.16	1.96	d_{xy}	this work
T^cPrP	^{t}BuNC	2.16	2.16	1.95	d_{xy}	this work
T^nPrP	^{t}BuNC	2.16	2.16	1.95	d_{xy}	this work
TPP	^{t}BuNC	2.18	2.18	1.93	d_{xy}	this work[b]
F_{20}-TPP	^{t}BuNC	2.31	2.31	1.86	d_{xy}	this work
OMTPP	^{t}BuNC	2.20	2.17	1.95	d_{xy}	this work
OETPP	^{t}BuNC	2.29	2.25	1.92	d_{xy}	this work
OEP	^{t}BuNC	2.29	2.29	1.86	d_{xy}	this work[c]
ProtoIXMe$_2$	^{t}BuNC	2.30	2.30	1.86	d_{xy}	this work

[a] The d_{xy} and d_π stand for the ground state with the $(d_{xz}, d_{yz})^4(d_{xy})^1$ and $(d_{xy})^2(d_{xz}, d_{yz})^3$ electron configurations, respectively. [b] Originally reported by Walker et al. at 77 K in frozen CH_2Cl_2; $g_1 = g_2 = 2.21$, $g_3 = 1.93$, ref 6. [c] Originally reported by Walker et al. at 77 K in frozen CH_2Cl_2; $g_1 = g_2 = 2.28$, $g_3 = 1.83$, ref 6.

Discussion

Solution Structure of $[Fe(TRP)L_2]^{\pm}$ and $[Fe(ORTPP)L_2]^{\pm}$. Before discussing the factors that affect the ground state electron configuration, we have examined the solution structure of the nonplanar porphyrin complexes. When the porphyrin ring is highly deformed, the planar ligands such as imidazole and pyridine tend to orient themselves along the cavities formed by the nonplanar porphyrin ring.[11,44] In the previous papers, we reported that the rotation of the coordinated 2-MeIm ligand in $[Fe(T^iPrP)(2\text{-MeIm})_2]^+$ is frozen on the ^1H NMR time scale at low temperature to show four pyrrole signals, two isopropyl methine signals, and four methyl signals.[12,18] Correspondingly, the ^{13}C NMR spectrum of the same complex exhibited four signals for the *β*-pyrrole carbon and two signals for the *meso* carbon as shown in Figure 4a; the α-pyrrole carbon also showed four signals between −6 and −90 ppm at −20 °C. These results suggest that the planar 2-MeIm ligands are fixed perpendicularly along the C(*meso*)−Fe−C(*meso*) axes, which in turn suggests that the porphyrin core in $[Fe(T^iPrP)L_2]^{\pm}$ is S_4-ruffled and creates the cavities along these axes in solution as shown in Figure 5a.[12] The result is consistent with the crystal structures of $[Fe(T^iPrP)(THF)_2]ClO_4$, in which porphyrin rings are highly S_4-ruffled.[35]

The porphyrin cores in $[Fe(ORTPP)L_2]^{\pm}$ are supposed to be S_4-saddled in solution, since the crystallographic analysis of the free bases $H_2(ORTPP)$ as well as their metal complexes always shows the strongly S_4-saddled porphyrin core.[25−28] In fact, Medforth and co-workers observed four signals for the methyl and *o*-phenyl protons in $[Co(OETPP)(3\text{-PhPy})_2]^+$.[45] The result was interpreted in terms of the mutually perpendicular alignment

(44) Walker, F. A.; Simonis, U. *J. Am. Chem. Soc.* **1991**, *113*, 8652−8657.
(45) Medforth, C. J.; Muzzi, C. M.; Shea, K. M.; Smith, K. M.; Abraham, R. J.; Jia, S.; Shelnutt, J. A. *J. Chem. Soc., Perkin Trans. 2* **1997**, 833−837.

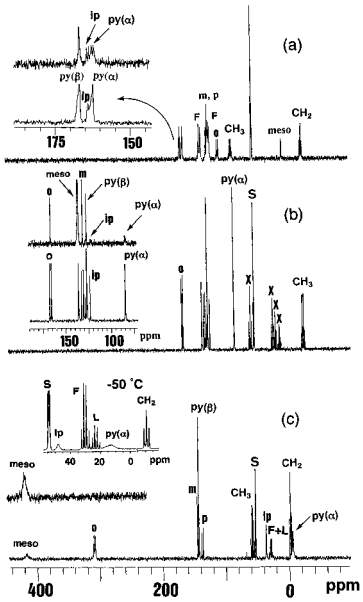

Figure 2. ^{13}C NMR spectra of (a) $[Fe(OETPP)(HIm)_2]^+$, (b) $[Fe(OMTPP)(CN)_2]^-$, and (c) $[Fe(OETPP)(^tBuNC)_2]^+$ taken in CD_2Cl_2 at 25 °C without decoupling of the proton region. ^{13}C NMR spectra of the *meso* ^{13}C enriched complexes taken under the broad band decoupling of the proton region are given in the insets of (a), (b), and (c). A part of the spectrum of $[Fe(OETPP)(^tBuNC)_2]^+$ taken at −50 °C is also given in the inset of (c). Signal assignment: o, m, p, and ip, *ortho*-, *meta*-, *para*-, and *ipso*-carbons; py(α) and py(*β*), α- and *β*-carbons of the pyrrole ring; L and F, methyl signal of the coordinated and free ^{t}BuNC ligand, respectively; s, dichloromethane; x, tetrabutylammonium ion. Note that both the py(α) and ipso(ip) carbon signals split into two signals in the *meso* ^{13}C enriched complexes as shown in the insets of (a) and (b).

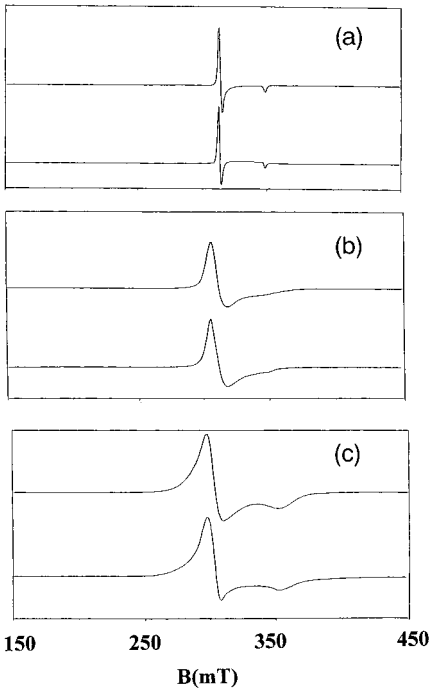

Figure 3. EPR spectra of (a) $[Fe(T^nPrP)(^tBuNC)_2]^+$, (b) $[Fe(OMTPP)(^tBuNC)_2]^+$, and (c) $[Fe(OETPP)(^tBuNC)_2]^+$. Bottom: observed spectra taken in frozen CH_2Cl_2 solution. Top: simulated spectra.

of the 3-PhPy ligands along the N−Co−N axes above and below the porphyrin ring. Thus, the porphyrin core in $[Co(OETPP)(3\text{-}PhPy)_2]^+$ maintains the S_4-saddled structure in solution and creates the cavities along these axes. It is then expected that

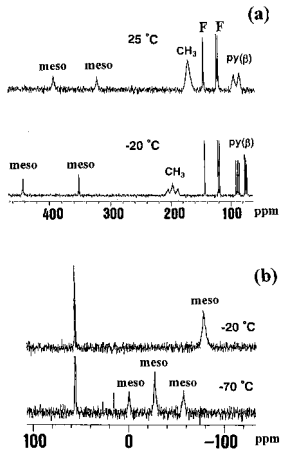

Figure 4. Temperature dependent ^{13}C NMR spectra of (a) $[Fe(T^iPrP)(2\text{-}MeIm)_2]^+$ [18] and (b) $[Fe(OETPP)(2\text{-}MeIm)_2]^+$ (*meso*-^{13}C enriched) taken in CD_2Cl_2 solution.

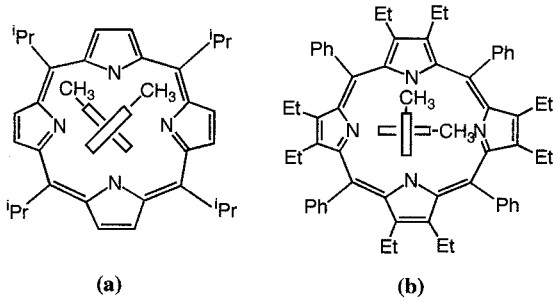

Figure 5. Orientation of the axially coordinated 2-MeIm ligands in (a) $[Fe(T^iPrP)(2\text{-}MeIm)_2]^+$ and (b) $[Fe(OETPP)(2\text{-}MeIm)_2]^+$.

the porphyrin cores in $[Fe(ORTPP)L_2]^{\pm}$ also maintain the strongly saddled structure in solution. To determine the porphyrin structure in solution, the NMR spectra of $[Fe(OETPP)(2\text{-}MeIm)_2]^+$ have been examined at low temperature. Although the ^1H NMR spectra of this complex showed the broadening and complicated splitting of the methyl, methylene, and phenyl signals below −80 °C due to the slow rotation of the coordinated 2-MeIm ligands, it was difficult to assign these signals under the present conditions (300 MHz NMR, −80 °C). Thus, we have examined the ligand orientation by means of the ^{13}C NMR spectra of *meso*-^{13}C enriched $[Fe(OETPP)(2\text{-}MeIm)_2]^+$. Figure 4b shows the ^{13}C NMR spectra of the *meso* carbon region. The *meso* signal appeared at δ −79.6 ppm at −20 °C, which broadened as the temperature was lowered and split into three signals below −60 °C. At −70 °C, three clearly separated signals were observed at $\delta = -0.6, -27.5$, and −57.5 ppm with the intensity ratios of 1:2:1, respectively. The result indicates that the axial ligands are fixed along the diagonal N−Fe−N axes on the ^{13}C NMR time scale as shown in Figure 5b, which in turn suggests that the strongly S_4-saddled structure is maintained in solution.[25−28] It should be noted that the hindered rotation of the 2-MeIm ligand was not observed even at −100 °C in the case of *meso*-^{13}C enriched $[Fe(OMTPP)(2\text{-}MeIm)_2]^+$. It seems to be strange that the rotational barrier of the 2-MeIm ligand in $[Fe(OETPP)(2\text{-}MeIm)_2]^+$ is greatly different from that in $[Fe(OMTPP)(2\text{-}MeIm)_2]^+$ despite the similar degree of nonplanarity expected for both complexes; the deviations of the py(*β*) carbon atoms from the average porphyrin plane in [Fe(OMTPP)Cl] and [Fe(OETPP)Cl] are 1.05 ± 0.10 Å and 1.15 ± 0.11 Å, respectivley.[28] The results could be explained if we assume the difference in rigidity of these complexes. In the ligand rotation process, the conformational

change of the nonplanar porphyrin ring should take place concomitantly to minimize the ligand−porphyrin repulsion.[46] Thus, the high barrier to ligand rotation in the OETPP complex relative to that in the OMTPP complex strongly suggests that the former is much more rigid than the latter. As discussed later, the rigidity of porphyrin ring plays an important role to determine the electron configuration.

Spectroscopic Methods to Determine the Electronic Ground State. We have already reported that, while $[Fe(THP)(CN)_2]^-$ and $[Fe(TPP)(CN)_2]^-$ have the common $(d_{xy})^2(d_{xz}, d_{yz})^3$ ground state,[13,43] $[Fe(TRP)(CN)_2]^-$ (R = ^{i}Pr, ^{c}Pr, and ^{n}Pr) adopt the less common $(d_{xz}, d_{yz})^4(d_{xy})^1$ ground state.[13,18] The difference in the electronic ground states between $[Fe(THP)(CN)_2]^-$ and $[Fe(TRP)(CN)_2]^-$ is mainly ascribed to the presence of the S_4-ruffled porphyrin cores in the latter complexes;[13] the S_4-ruffling makes the interaction between the iron d_{xy} and porphyrin a_{2u} orbitals possible and raises the energy level of the d_{xy} orbital as Walker, Debrunner, Scheidt, and co-workers pointed out.[4] This mode of porphyrin deformation, therefore, stabilizes the $(d_{xz}, d_{yz})^4(d_{xy})^1$ state relative to the $(d_{xy})^2(d_{xz}, d_{yz})^3$ state. The difference in orbital interactions in the $(d_{xy})^2(d_{xz}, d_{yz})^3$ and $(d_{xz}, d_{yz})^4(d_{xy})^1$ type complexes could induce a large change in spin densities at the porphyrin carbon and nitrogen atoms. In fact, our recent studies using $[Fe(TRP)L_2]^{\pm}$ have revealed that the major spin densities in the $(d_{xz}, d_{yz})^4(d_{xy})^1$ type complexes are at the *meso* carbon and pyrrole nitrogen atoms; these atoms have 0.045 and 0.057 electrons, respectively, in the case of $[Fe(T^iPrP)(4\text{-}CNPy)_2]^+$.[18] The large spin densities at the *meso* carbon atoms is one of the characteristic features of the $(d_{xz}, d_{yz})^4(d_{xy})^1$ type complexes; the recent spectroscopic studies have revealed that not only the *meso*-substituted complexes such as $[Fe(TRP)(4\text{-}CNPy)_2]^+$ and $[Fe(TArP)(CN)_2]^-$,[18,43] but also the *meso*-unsubstituted $[Fe(OEP)(^tBuNC)_2]^+$, have large spin densities at the *meso* carbon atoms.[6] Thus, the spin distribution in the $(d_{xz}, d_{yz})^4(d_{xy})^1$ type complexes differs from that in the $(d_{xy})^2(d_{xz}, d_{yz})^3$ type complexes where the major spin densities are at the β-pyrrole carbon atoms.[47−52]

The difference in spin distribution results in the extremely different NMR spectra. The ^{1}H NMR characteristics of the $(d_{xz}, d_{yz})^4(d_{xy})^1$ type complexes as compared with those of the $(d_{xy})^2(d_{xz}, d_{yz})^3$ type complexes have been extensively studied. They are summarized as follows:[1−4,6,8,9,11−18,43] (i) the downfield shift of the *meso*-CH and *meta*-H signals in TRP and TArP complexes, respectively, (ii) the upfield shift of the *meso*-H in OEP complexes, and (iii) the downfield shifts of the py-H signals. While the characteristics (i) and (ii) are originated from the large spin densities at the *meso* carbons, (iii) is ascribed to the smaller spin densities at the py(β) carbons in the $(d_{xz}, d_{yz})^4(d_{xy})^1$ type complexes. The sign reversal in dipolar shift also contributes to the downfield shift of the py-H signals.[1,18]

In principle, ^{13}C NMR chemical shifts can be a better probe to determine the electronic ground state, because they give the information on the spin distribution of any porphyrin carbons including *meso*, py(α), and py(β) regardless of the substituent positions at the porphyrin periphery. In fact, we have established that not only the *meso* carbon but also the py(α) carbon signals appear at the characteristic positions in the $(d_{xz}, d_{yz})^4(d_{xy})^1$ type complexes; they appear at extremely downfield and upfield positions, respectively.[11,14,18] In the case of $[Fe(T^iPrP)(4\text{-}CNPy)_2]^+$, for example, the *meso* and py(α) carbon signals were observed at 918 and −295 ppm at −50 °C, respectively.[18] The large upfield shift of the py(α) carbon signal can be explained in terms of the spin polarization effect from the *meso* carbon and pyrrole nitrogen atoms; these atoms have the largest spin densities in the $(d_{xz}, d_{yz})^4(d_{xy})^1$ type complexes. More importantly, we can compare the contribution of the $(d_{xz}, d_{yz})^4(d_{xy})^1$ state to the electronic ground state in a wide variety of complexes such as TRP, TPP, ORTPP, OEP, and ProtoIXMe$_2$ on the basis of the chemical shifts of these carbon atoms; the comparison of the ^{1}H NMR chemical shifts is sometimes hampered because some complexes have no protons at the *meso* and/or β-pyrrole positions.

The ground-state electron configuration determined on the basis of the ^{13}C NMR and ^{1}H NMR spectra was further confirmed by the types of the EPR spectra; the axial type EPR spectra correspond to the complexes with the $(d_{xz}, d_{yz})^4(d_{xy})^1$ ground state while the large g_{max} or rhombic type spectra to those with the $(d_{xy})^2(d_{xz}, d_{yz})^3$ ground state.[53,54]

Ground-State Electron Configuration. As mentioned in the Introduction, the axial ligands examined in this study are typical bases to form the low-spin Fe(III) porphyrin complexes. The electronic effect of these ligands on the Fe(III) ion is, however, quite different. Although imidazole and cyanide are strong σ-donors, the π-accepting abilities of these ligands are different; cyanide is a much stronger π-acceptor than imidazole.[55,56] In contrast, *tert*-butyl isocyanide is classified as a weak σ-donor and a strong π-acceptor.[2,6] We have measured the ^{1}H NMR, ^{13}C NMR, and EPR spectra of the complexes having these ligands at the axial positions and examined how the ground state of the low-spin complexes changes depending upon the structural and electronic differences of the porphyrin ring.

(i) Bis(imidazole) Complexes. (a) $[Fe(TRP)(HIm)_2]^+$ (R = ^{i}Pr, ^{c}Pr, ^{n}Pr). The electronic ground state of these complexes has been reported in our previous paper on the basis of the NMR and EPR spectra.[18] Only the isopropyl complex $[Fe(T^iPrP)(HIm)_2]^+$ adopts the $(d_{xz}, d_{yz})^4(d_{xy})^1$ ground state; the ^{c}Pr and ^{n}Pr complexes showed the common $(d_{xy})^2(d_{xz}, d_{yz})^3$ ground state. It should be noted that the electronic effects of the propyl, cyclopropyl, and isopropyl groups are considered to be quite similar. Thus, the difference in the electron configuration among three complexes should be ascribed to the degree of nonplanarity of the porphyrin rings. That is, the S_4-ruffling of the porphyrin structure affects the electron configuration and stabilizes the $(d_{xz}, d_{yz})^4(d_{xy})^1$ state.

(b) $[Fe(TPP)(HIm)_2]^+$. This complex shows the $(d_{xy})^2(d_{xz}, d_{yz})^3$ ground state as revealed from the large upfield shift of the pyrrole proton signal as well as the rhombic EPR spectrum.[53,57,58]

(46) Saitoh, T.; Ikeu, T.; Ohgo, Y.; Nakamura, M. *Tetrahedron* **1997**, *53*, 12487−12496.
(47) Wüthrich, K.; Baumann, R. *Helv. Chim. Acta* **1973**, *56*, 585−596.
(48) Wüthrich, K.; Baumann, R. *Helv. Chim. Acta* **1974**, *57*, 336−350.
(49) La Mar, G. N.; Viscio, D. B.; Smith, K. M.; Caughey, W. S.; Smith, M. L. *J. Am. Chem. Soc.* **1978**, *100*, 8085−8092.
(50) Goff, H. M. *J. Am. Chem. Soc.* **1981**, *103*, 3714−3722.
(51) Goff, H. M. Nuclear Magnetic Resonance of Iron Porphyrins. In *Iron Porphyrin, I*; Lever, A. B. P., Gray, H. B., Eds.; Addison-Wesley: Reading, MA, 1983; Physical Bioinorganic Chemistry Series 1, pp 237−281.
(52) Bertini, I.; Luchinat, C. NMR of Paramagnetic Substances. In *Coordination Chemistry Reviews 150*; Lever, A. B. P., Ed.; Elsevier: Amsterdam, 1996; pp 29−75.
(53) Walker, F. A.; Reis, D.; Balke, V. L. *J. Am. Chem. Soc.* **1984**, *106*, 6888−6898.
(54) Walker, F. A.; Reis, D.; Balke, V. L. *J. Am. Chem. Soc.* **1986**, *108*, 5288−5297.
(55) Shriver, D. F.; Atkins, P. W.; Langford, C. H. In *Inorganic Chemistry*, 2nd ed.; Oxford University Press: Oxford, 1994; pp 246−261.
(56) Frye, J. S.; La Mar, G. N. *J. Am. Chem. Soc.* **1975**, 97, 3561−3562.
(57) Satterlee, J. D.; La Mar, G. N. *J. Am. Chem. Soc.* **1976**, *98*, 2804−2808.

(c) [Fe(ORTPP)(HIm)$_2$]$^+$ (R = Me, Et). Table 1 shows the existence of the downfield shifted methyl and methylene signals in [Fe(OMTPP)(HIm)$_2$]$^+$ and [Fe(OETPP)(HIm)$_2$]$^+$, respectively. The results suggest that the β-pyrrole carbons have a considerable amount of spin densities, which is one of the characteristic features of the complexes having the $(d_{xy})^2(d_{xz}, d_{yz})^3$ ground state.[50] Similarity of the chemical shifts of the phenyl protons in [Fe(ORTPP)(HIm)$_2$]$^+$ and [Fe(TPP)(HIm)$_2$]$^+$ also supports the $(d_{xy})^2(d_{xz}, d_{yz})^3$ ground state. The assignment was further confirmed by the EPR spectra; both complexes exhibited the rhombic spectra as in the case of [Fe(TPP)(HIm)$_2$]$^+$.[53,58] However, the ^{13}C NMR chemical shifts in Table 2 show some deviations from those of [Fe(TPP)(HIm)$_2$]$^+$. The major difference lies in the chemical shifts of the py(α) and py(β) carbon atoms. While the chemical shifts of the py(α) and py(β) of [Fe(TPP)(HIm)$_2$]$^+$ were -2.0 and 77.1 ppm at -50 °C, respectively, those of the corresponding carbons in [Fe(OETPP)(HIm)$_2$]$^+$ were 143.5 and 156.1 ppm. The chemical shifts of the *meso* carbon atoms also showed some difference; they were 25.2 and -37.2 ppm for [Fe(TPP)(HIm)$_2$]$^+$ and [Fe(OETPP)(HIm)$_2$]$^+$, respectively. The results might be the indication that the iron(d_π) and porphyrin(p_π) interactions are perturbed by the S_4-saddled deformation of the porphyrin ring, which will be discussed in the latter part of this paper.

(ii) Bis(cyanide) Complexes. (a) [Fe(TRP)(CN)$_2$]$^-$ (R = ^{i}Pr, ^{c}Pr, ^{n}Pr). Ground-state electron configuration of these complexes has already been determined as $(d_{xz}, d_{yz})^4(d_{xy})^1$ in our previous papers.[13,18] The chemical shifts of the pyrrole proton and the *meso* carbon atoms in these complexes clearly indicate that the contribution of the $(d_{xz}, d_{yz})^4(d_{xy})^1$ state to the electronic ground state increases in the following order: [Fe(T^{n}PrP)(CN)$_2$]$^-$ $\leq$ [Fe(T^{c}PrP)(CN)$_2$]$^-$ $<$ [Fe(T^{i}PrP)(CN)$_2$]$^-$. Since the electronic effects of the alkyl groups on the porphyrin ring are considered to be quite similar, the increase in the $(d_{xz}, d_{yz})^4(d_{xy})^1$ contribution should again be ascribed to the degree of S_4-ruffling of the porphyrin ring.

(b) [Fe(TPP)(CN)$_2$]$^-$. Electron configuration of this complex was determined to be $(d_{xy})^2(d_{xz}, d_{yz})^3$ on the basis of the ^{1}H NMR, ^{13}C NMR, and EPR spectroscopic data.[42,43]

(c) [Fe(ORTPP)(CN)$_2$]$^-$ (R = Me, Et). The ^{1}H NMR chemicals shifts in Table 1 indicate that both [Fe(OMTPP)(CN)$_2$]$^-$ and [Fe(OETPP)(CN)$_2$]$^-$ adopt the common $(d_{xy})^2(d_{xz}, d_{yz})^3$ ground state. The large downfield shifts of the methyl and methylene signals in these complexes correspond to the large upfield shift of the pyrrole protons in [Fe(TPP)(CN)$_2$]$^-$, suggesting that the major spin densities are at the β-pyrrole carbon atoms. The ^{13}C NMR chemical shifts in Table 2 also support this configuration because the *meso* carbon signals appeared rather upfield, 87.4 and 45.1 ppm, respectively. The large g_{max}-type EPR spectra observed for these complexes are the direct evidence for the $(d_{xy})^2(d_{xz}, d_{yz})^3$ configuration; the *g* values are 3.48 and 3.31 as listed in Table 3. The downfield shifts of the α- and β-pyrrole carbon signals were again observed in [Fe(OETPP)(CN)$_2$]$^-$; the chemical shifts were 128.8 and 142.4 ppm, respectively, as compared with 18.2 and 86.2 ppm in [Fe(TPP)(CN)$_2$]$^-$.

(iii) Bis(*tert*-butyl isocyanide) Complexes. (a) [Fe(TRP)(^{t}BuNC)$_2$]$^+$ (R = ^{i}Pr, ^{c}Pr, ^{n}Pr). The low-spin Fe(III) complexes consisting of the S_4-ruffled porphyrin ring and the weak axial ligands with low lying p_{π^*} orbitals are expected to have a very pure $(d_{xz}, d_{yz})^4(d_{xy})^1$ ground state. In fact, the data in Table 1 indicate that both the pyrrole and *meso* α-proton signals moved downfield on going from [Fe(TRP)(HIm)$_2$]$^+$ to [Fe(TRP)(CN)$_2$]$^-$ and then to [Fe(TRP)(^{t}BuNC)$_2$]$^+$. In the case of the ^{n}Pr complexes, the chemical shift of the *meso* α-proton changed from 1.72 to 30.91 and then to 118.5 ppm at -50 °C. The results suggest that the spin densities at the *meso* carbons have increased to a great extent as the axial HIm is replaced by ^{t}BuNC. As mentioned, the ^{13}C NMR spectra of a series of [Fe(TRP)(^{t}BuNC)$_2$]$^+$ showed neither the *meso* carbon nor the py(α) carbon signals even at 25 °C. The results indicate that both the *meso* and py(α) carbons have very short relaxation times, which must be ascribed to the fairly large spin densities at the *meso* carbon and pyrrole nitrogen atoms.[18] The EPR spectra of these complexes showed clear axial type signals. Figure 3a demonstrates the EPR spectrum of [Fe(T^{n}PrP)(^{t}BuNC)$_2$]$^+$ as a typical example. The *g* values were determined to be $g_\perp = 2.16$ and $g_{||} = 1.95$. On the basis of the ^{1}H NMR, ^{13}C NMR, and EPR results, it is clear that the [Fe(TRP)(^{t}BuNC)$_2$]$^+$ (R = ^{n}Pr, ^{c}Pr, or ^{i}Pr) complexes have a very pure $(d_{xz}, d_{yz})^4(d_{xy})^1$ ground state.

(b) [Fe(TPP)(^{t}BuNC)$_2$]$^+$. The ground-state electron configuration of this complex was already determined as $(d_{xz}, d_{yz})^4(d_{xy})^1$.[2,6] The coordination of the weak axial ligand stabilizes the iron $d_\pi(d_{xz}, d_{yz})$ orbitals to the point lower than or equal to the d_{xy} orbital.[6,7] In this situation, if the normally planar TPP ring deforms in a S_4-ruffled fashion, further stabilization can be obtained by the iron d_{xy} and porphyrin a_{2u} interaction, inducing the less common $(d_{xz}, d_{yz})^4(d_{xy})^1$ configuration. In fact, the porphyrin core of this complex is reported to be strongly S_4-ruffled as revealed by the X-ray crystallographic analysis.[6] The ^{13}C NMR data listed in Table 2 also support this conclusion; the chemical shifts of the *meso* and α-pyrrole carbons were estimated to be 997 and -429 ppm, respectively, at -50 °C.

(c) [Fe(ORTPP)(^{t}BuNC)$_2$]$^+$ (R = Me, Et). The similarity of the phenyl proton chemical shifts in [Fe(OMTPP)(^{t}BuNC)$_2$]$^+$ and [Fe(TPP)(^{t}BuNC)$_2$]$^+$ suggests that the ground-state electron configuration of the former complex is also represented as $(d_{xz}, d_{yz})^4(d_{xy})^1$. The conclusion is further supported by the presence of the extremely downfield and upfield shifted *meso* and py(α) carbon signals, respectively; these signals appeared at 979 and -377 ppm at -50 °C. The ^{13}C NMR spectra of [Fe(OETPP)(^{t}BuNC)$_2$]$^+$ also showed the downfield and upfield shifted *meso* and py(α) signals, respectively. The chemical shifts of these signals are, however, markedly different from those of [Fe(OMTPP)(^{t}BuNC)$_2$]$^+$; the *meso* and the py(α) signals were observed at 416 and 13.3 ppm, respectively, at -50 °C. These results suggest that the spin densities at the *meso* carbon atoms in [Fe(OETPP)(^{t}BuNC)$_2$]$^+$ are much smaller than those of the analogous [Fe(OMTPP)(^{t}BuNC)$_2$]$^+$. On the basis of the NMR results, the following two points have become clear for [Fe(OMTPP)(^{t}BuNC)$_2$]$^+$ and [Fe(OETPP)(^{t}BuNC)$_2$]$^+$: (i) the ground states of both complexes are represented mainly as the $(d_{xz}, d_{yz})^4(d_{xy})^1$ state and (ii) the contribution of the $(d_{xz}, d_{yz})^4(d_{xy})^1$ state to the electronic ground state is much larger in [Fe(OMTPP)(^{t}BuNC)$_2$]$^+$ than in [Fe(OETPP)(^{t}BuNC)$_2$]$^+$. The assignment of the ground-state electron configuration of all the complexes examined in this study is listed in Table 3, where the d_{xy} and d_π stand for the $(d_{xz}, d_{yz})^4(d_{xy})^1$ and $(d_{xy})^2(d_{xz}, d_{yz})^3$ ground states, respectively.

Factors Affecting the Electronic Ground State. (i) Axial Ligands. Effects of axial ligands on the ground state electron configuration of the low-spin Fe(III) porphyrin complexes have been studied extensively in [Fe(TPP)L$_2$]$^+$ and [Fe(TRP)L$_2$]$^+$.[3,18] The present results are consistent with the previous ones in the sense that the contribution of the $(d_{xz}, d_{yz})^4(d_{xy})^1$ state increases

(58) La Mar, G. N.; Walker, F. A. *J. Am. Chem. Soc*. **1973**, *95*, 1782−1790.

on going from $[Fe(Porphyrin)(Him)_2]^+$ to $[Fe(Porphyrin)(CN)_2]^-$ and then to $[Fe(Porphyrin)(^tBuNC)_2]^+$. In other words, the $(d_{xz}, d_{yz})^4(d_{xy})^1$ character increases as the σ-donating ability of ligands is weakened and π-accepting ability is strengthened.

(ii) Deformation Mode of Porphyrins. We have reported that the electron configuration of $[Fe(TRP)(CN)_2]^-$ changes from $(d_{xy})^2(d_{xz}, d_{yz})^3$ to $(d_{xz}, d_{yz})^4(d_{xy})^1$ as the bulkiness of alkyl substituents increases. Since the electronic effects of these groups on the porphyrin ring are considered to be quite similar, the result has been ascribed to the increase in magnitude of the S_4-ruffled structure.[13]

It is much more difficult to elucidate the effect of S_4-saddled structure on the electronic ground state. This is because both geometry and electronic structure of porphyrin ring change on going from the planar TPP to the S_4-saddled ORTPP ligand. Thus, we have to find a suitable model complex in which porphyrin ring is S_4-saddled, while the electronic structure of porphyrin is similar to that of the planar complex. Although it is very difficult to find such model complexes, we can extract some information from the ^{13}C NMR chemical shifts of $[Fe(TPP)(^tBuNC)_2]^+$, $[Fe(OMTPP)(^tBuNC)_2]^+$, and $[Fe(OETPP)(^tBuNC)_2]^+$ listed in Table 2. The chemical shifts of the py(α), py(β), and *meso* carbons showed only a small change on going from $[Fe(TPP)(^tBuNC)_2]^+$ to $[Fe(OMTPP)(^tBuNC)_2]^+$; they are -429, 60, 997 ppm in the former and -377, 90, 979 ppm in the latter complex, respectively. The introduction of the eight methyl groups at the β-pyrrole carbons apparently gives only a little influence on the chemical shifts of the porphyrin carbon atoms. The similarity of the ^{13}C NMR chemical shifts between $[Fe(TPP)(^tBuNC)_2]^+$ and $[Fe(OMTPP)(^tBuNC)_2]^+$ should be considered, however, to be the result of the two different factors: (i) change in porphyrin structure caused by the steric effects of the eight methyl groups and (ii) change in electronic structure caused by the electron donation of the eight methyl groups. Surprisingly, the introduction of the eight ethyl groups changed the chemical shifts of the py(α), py(β), and *meso* carbons to a great extent; they are 13, 136, and 416 ppm, respectively, in $[Fe(OETPP)(^tBuNC)_2]^+$. Since the electron donating ability of ethyl group is similar to that of methyl group, the large difference in chemical shifts observed between $[Fe(OMTPP)(^tBuNC)_2]^+$ and $[Fe(OETPP)(^tBuNC)_2]^+$ is caused by the difference in steric effects of these groups. We ascribe the results to the rigidity of porphyrin ring in $[Fe(OETPP)(^tBuNC)_2]^+$ as compared with that in $[Fe(OMTPP)(^tBuNC)_2]^+$. In both complexes, the $(d_{xz}, d_{yz})^4(d_{xy})^1$ state is stabilized by the $a_{2u}-d_{xy}$ interaction if the porphyrin ring could deform in a S_4 ruffled fashion. However, the OETPP core is much more rigid than the OMTPP core as revealed from the high barrier to rotation of the coordinated 2-MeIm ligand; the *meso* carbons of $[Fe(OETPP)(2\text{-}MeIm)_2]^+$ showed three signals below -50 °C as shown in Figure 4b, while those of $[Fe(OMTPP)(2\text{-}MeIm)_2]^+$ maintained singlet even at -100 °C. The rigidity of the OETPP core is also reflected on the barrier to inversion of the deformed porphyrin ring; the inversion barrier of [Fe(OETPP)Cl] is estimated to be 15.7−16.0 kcal mol^{-1} as compared with 10.1−10.5 kcal mol^{-1} in [Fe(OMTPP)Cl].[28,59] Thus, the contribution of the $(d_{xz}, d_{yz})^4(d_{xy})^1$ state on the electronic ground state is smaller in $[Fe(OETPP)(^tBuNC)_2]^+$ than in $[Fe(OMTPP)(^tBuNC)_2]^+$ since much more energy is required for the ruffling of the OETPP core. Consequently, the isotropic shifts of the py(α) and *meso* carbon signals are smaller than those of $[Fe(OMTPP)(^tBuNC)_2]^+$. On the basis of these results, we conclude that the low-spin iron(III) complexes with the saddle shaped structure resist to switch the electronic ground state from the common $(d_{xy})^2(d_{xz}, d_{yz})^3$ to the less common $(d_{xz}, d_{yz})^4(d_{xy})^1$.[60,61]

The conclusion mentioned above can be explained as follows. In the S_4 saddled complexes, the $a_{2u}-d_{xy}$ interaction is weakened as compared with that in the S_4 ruffled ones. In contrast, the $3e_g-d_\pi$ interaction is expected to be strengthened due to the short metal-nitrogen bond lengths[27,28] as well as the efficient overlap between the $3e_g$ and d_π orbitals. The large downfield shifts of the α- and β-pyrrole signals observed in the saddled complexes could be ascribed to this interaction since the $3e_g$ orbitals have electron densities at the α- and β-pyrrole carbon atoms. Thus, the $(d_{xy})^2(d_{xz}, d_{yz})^3$ state is stabilized relative to the $(d_{xz}, d_{yz})^4(d_{xy})^1$ state as the porphyrin ring changes from the planar to the saddled structure.

As is well-known, ^{t}BuNC is the ligand to stabilize the $(d_{xz}, d_{yz})^4(d_{xy})^1$ ground state.[2,6] In fact, all the complexes examined in this study showed the $(d_{xz}, d_{yz})^4(d_{xy})^1$ ground state. On the basis of the EPR g values listed in Table 3, the energy parameters Δ and V were calculated. In the case of $[Fe(T^nPrP)(^tBuNC)_2]^+$, the Δ and V values were $-10.7\ \lambda$ and $0.0\ \lambda$, respectively, in units of the spin−orbit coupling constant λ.[62−64] The results indicate that the d_{xy} orbital is located $10.7\ \lambda$ above the degenerated d_{xz} and d_{yz} orbitals. In the case of $[Fe(T^iPrP)(^tBuNC)_2]^+$, the $|\Delta|$ value reached as much as $11.3\ \lambda$, which is one of the largest values ever reported for the low-spin Fe(III) porphyrin complexes.[65−67] Figure 6 shows the relative energy differences among three d orbitals. Thus, the contribution of the $(d_{xz}, d_{yz})^4(d_{xy})^1$ state increases in the following order at 4.2 K in the case of the bis(^{t}BuNC) complexes:

$$OETPP < OMTPP, TPP < T^nPrP, T^cPrP, T^iPrP$$

Similar order is established on the basis of the ^{13}C NMR *meso* shifts. The ^{13}C NMR data reported in this and in our previous papers indicate that the complexes showing the *meso*-carbon signals below 300 ppm, $\delta > 300$, exhibit the axial type EPR spectra though the temperatures examined are greatly different between two methods: 4.2 K in EPR vs 223 K in ^{13}C NMR.[18,43] The result could be the indication that, when the $(d_{xz}, d_{yz})^4(d_{xy})^1$ contribution exceeds a threshold value, e.g., δ 300 ppm for

(59) Nakamura, M.; Yamaguchi, T.; Ohgo, Y. *Inorg. Chem.* **1999**, *38*, 3857−3862.

(60) One of the reviewers pointed out that saddling is invariably accompanied by ruffling of the porphyrin core as in the case of [Fe(OMTPP)Cl] and [Fe(OETPP)Cl],[28] and that it is not possible to separate the effects of saddling and ruffling. However, our preliminary result on the X-ray crystallographic analysis of $[Fe(OETPP)Py_2]ClO_4$ has revealed that the OETPP ring is essentially saddle shaped; the rotation of the pyrrole planes with respect to the mean porphyrin plane are at most 3°.[61] Obviously, an extensive crystallographic study including the structural comparison of $[Fe(OMTPP)L_2]ClO_4$ and $[Fe(OETPP)L_2]ClO_4$ for various axial ligands (L's) is necessary for the better understanding of the effect of the deformation mode of porphyrin ring on the electronic ground state, which is now in progress in this laboratory.

(61) Ohgo, Y.; Ikeue, T.; Nakamura, M. To be published.
(62) Taylor, C. P. S. *Biochim. Biophys. Acta* **1977**, *491*, 137−149.
(63) Bohan, T. L. *J. Magn. Reson.* **1977**, *26*, 109−118.
(64) Palmer, G. Electron Paramagnetic Resonance of Hemoproteins. In *Iron Porphyrins, Part II.*; Lever, A. B. P., Gray, H. B., Eds.; Addison-Wesley: Reading, MA, 1983; Physical Bioinorganic Chemistry Series 2, pp 43−88.

(65) A couple of papers have appeared recently describing the formation of the complex with very pure $(d_{xz}, d_{yz})^4(d_{xy})^1$ configuration.[66,67]

(66) Moore, K. T.; Fletcher, J. T.; Therien, M. J. *J. Am. Chem. Soc.* **1999**, *121*, 5196−5209.
(67) Simonneaux, G.; Schünemann, V.; Morice, C.; Carel, L.; Toupet, L.; Winler, H.; Trautwein, A. X.; Walker, F. A. *J. Am. Chem. Soc.* **2000**, 122, 4366−4377.

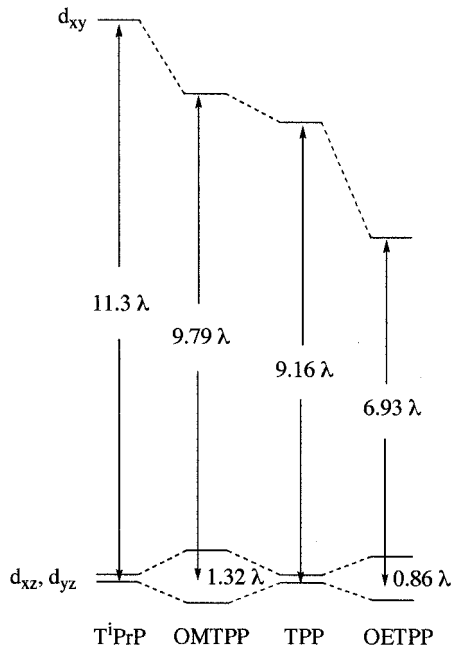

Figure 6. Relative energy levels of the three d orbitals in a series of [Fe(Porphyrin)(^{t}BuNC)$_2$]$^+$ represented in units of spin−orbit coupling constant λ, where Porphyrins are T^{i}PrP, OMTPP, TPP, and OETPP.

meso carbon at 223 K, the electronic ground-state falls into the $(d_{xz}, d_{yz})^4(d_{xy})^1$ type at 4.2 K, giving the axial type EPR spectra. In the case of the bis(CN^-) and bis(HIm) complexes, the following order has been established on the basis of the ^{13}C and ^1H NMR chemical shifts:

$$\text{OETPP} \leq \text{OMTPP} \leq \text{TPP} < \text{T}^n\text{PrP}, \text{T}^c\text{PrP} < \text{T}^i\text{PrP}$$

In any case, the $(d_{xz}, d_{yz})^4(d_{xy})^1$ contribution is the smallest in the saddled OETPP complexes and the largest in the ruffled T^{i}PrP complexes. The rhombic EPR spectra observed in [Fe(OMTPP)(^{t}BuNC)$_2$]$^+$ and [Fe(OETPP)(^{t}BuNC)$_2$]$^+$ indicate that the energy levels of the d_{xz} and d_{yz} orbitals are different as shown in Figure 6. The results suggest that the four Fe−N(porphyrin) bonds are no longer equivalent in frozen CH_2Cl_2 solution at 4.2 K;[30,68] they are equivalent if porphyrin core is S_4-saddled. This might be the indication that both [Fe(OMTPP)(^{t}BuNC)$_2$]$^+$ and [Fe(OETPP)(^{t}BuNC)$_2$]$^+$ have saddle shaped structure with some ruffled deformation.[20,30] The V values of [Fe(OMTPP)(^{t}BuNC)$_2$]$^+$ and [Fe(OETPP)(^{t}BuNC)$_2$]$^+$, 1.32λ and 0.86λ, respectively, indicate that the magnitude of ruffling is larger in the former complex than in the latter, suggesting the less rigidity in the OMTPP ring.

(iii) a_{1u} and a_{2u} HOMOs. It is well-known that the porphyrin HOMO is either a_{1u} or a_{2u} depending on the positions and the electronic nature of substituents.[36,69] All the low-spin complexes so far discussed have *meso*-substituted porphyrins with a_{2u} HOMO, i.e., TRP,[36] TPP,[36,70−72] and ORTPP,[27,59] as revealed from the EPR and ^1H NMR spectra of the corresponding radical cations. We have then examined the low-spin complexes where the porphyrins have a_{1u} HOMO. Such porphyrins are OEP and ProtoIXMe$_2$.[36] Walker, Debrunner, Scheidt, and co-workers have reported that [Fe(OEP)(^{t}BuNC)$_2$]$^+$ has the $(d_{xz}, d_{yz})^4(d_{xy})^1$ ground state on the basis of the ^1H NMR, EPR, Mössbauer, and X-ray crystallography.[6] We have examined the complexes such as [Fe(OEP)(^{t}BuNC)$_2$]$^+$ and [Fe(ProtoIXMe$_2$)(^{t}BuNC)$_2$]$^+$, focusing our attention on how much the $(d_{xz}, d_{yz})^4(d_{xy})^1$ state contributes to the electronic ground state. The ^1H NMR spectra of [Fe(ProtoIXMe$_2$)(^{t}BuNC)$_2$]$^+$ taken at −50 °C showed the *meso* signals fairly upfield, −70.4 and −71.6 ppm. These values are close to −58.2 ppm in [Fe(OEP)(^{t}BuNC)$_2$]$^+$. The results clearly indicate that [Fe(ProtoIXMe$_2$)(^{t}BuNC)$_2$]$^+$ also adopts the $(d_{xz}, d_{yz})^4(d_{xy})^1$ ground state; the *meso* signals in the $(d_{xy})^2(d_{xz}, d_{yz})^3$ type complexes appear at δ ca. 5 ppm.[51] The ^1H NMR method is difficult, however, to rank the $(d_{xz}, d_{yz})^4(d_{xy})^1$ contribution in a variety of complexes, since the porphyrins with a_{2u} HOMO have no protons at the *meso* positions. Thus, we examined the ^{13}C NMR spectra of these complexes. The chemical shifts of the *meso* carbons were 767, 419, and 396 ppm at 25 °C for the TPP, OEP, and ProtoIXMe$_2$ complexes, respectively, indicating that the $(d_{xz}, d_{yz})^4(d_{xy})^1$ contribution is much larger in the TPP complex than in the OEP and ProtoIXMe$_2$ complexes. The EPR g values obtained at 4.2 K are consistent with the NMR chemical shifts at −50 °C; the $|\Delta|$ values for the TPP, OEP, and ProtoIXMe$_2$ complexes are 9.16, 5.73, and 5.63 λ, respectively, Thus, the $(d_{xz}, d_{yz})^4(d_{xy})^1$ contribution in these complexes is as small as that of the OETPP complexes.

The results mentioned above indicate that the complexes with a_{1u} HOMO tend to maintain the $(d_{xy})^2(d_{xz}, d_{yz})^3$ state even for the axial ligands which prefer the $(d_{xz}, d_{yz})^4(d_{xy})^1$ state. This is because, the a_{1u} HOMO has small spin densities at the pyrrole nitrogens. Thus, the participation of this orbital to the charge-transfer becomes fairly small. In contrast, the a_{2u} HOMO has large spin densities at the pyrrole nitrogens and *meso* carbons and can directly participate in charge transfer when the porphyrin is ruffled. Thus, the electron donating alkyl groups at the *meso* positions destabilize the a_{2u} orbital and strengthen the $a_{2u}-d_{xy}$ interactions.

(iv) Electronic Effects of Peripheral Substituents. As we have just mentioned, the introduction of the electron donating alkyl substituents to the *meso* positions increases the $(d_{xz}, d_{yz})^4(d_{xy})^1$ contribution. It is then expected that the electron withdrawing groups at the *meso* positions stabilizes the a_{2u} orbital and decreases the $(d_{xz}, d_{yz})^4(d_{xy})^1$ contribution. To confirm this hypothesis, we have examined the ^1H NMR spectra of [Fe(F$_{20}$-TPP)L$_2$]$^\pm$ (L = HIm, CN^-, and ^{t}BuNC) and compared the chemical shifts with those of the parent [Fe(TPP)L$_2$]$^\pm$ (L = HIm, CN^-, and ^{t}BuNC). The pyrrole signals of [Fe(F$_{20}$-TPP)L$_2$]$^\pm$ were observed at −24.4, −32.5, and +5.48 ppm at −50 °C for L = HIm, CN^-, and ^{t}BuNC, respectively, as compared with −26.1, −28.7, and +11.7 ppm in [Fe(TPP)L$_2$]$^\pm$. Especially important is the difference in chemical shifts between [Fe(F$_{20}$-TPP)(^{t}BuNC)$_2$]$^+$ and [Fe(TPP)(^{t}BuNC)$_2$]$^+$; +5.48 ppm for the former and +11.7 ppm for the latter complex. Since both of these complexes adopt the $(d_{xz}, d_{yz})^4(d_{xy})^1$ ground state, the pyrrole proton chemical shifts suggest that the $(d_{xz}, d_{yz})^4(d_{xy})^1$ contribution is much larger in [Fe(TPP)(^{t}BuNC)$_2$]$^+$. The ^1H NMR result is further supported by the EPR result; the $g_\perp$ and $g_{||}$ values of [Fe(TPP)(^{t}BuNC)$_2$]$^+$ are 2.18 and 1.93, respectively, while those of [Fe(F$_{20}$-TPP)(^{t}BuNC)$_2$]$^+$ are 2.31 and 1.86. Similar results have already been reported by our previous paper on the electron configuration of

(68) Ochsenbein, P.; Mandon, D.; Fischer, J.; Weiss, R.; Austin, R.; Jayaraj, K.; Gold, A.; Terner, J.; Bill, E.; Muther, M.; Trautwein, A. X. *Angew. Chem., Int. Ed. Engl.* **1993**, *32*, 1437−1438.
(69) Jayaraj, K.; Terner, J.; Gold, A.; Roberts, D. A.; Austin, R. N.; Mandon, D.; Weiss, R.; Bill, E.; Müther, M.; Trautwein, A. X. *Inorg. Chem.* **1996**, *35*, 1632−1640.
(70) Goff, H. M.; Phillippi, M. A. *J. Am. Chem. Soc.* **1983**, *105*, 7567−7571.
(71) Boersma, A. D.; Goff, H. M. *Inorg. Chem.* **1984**, *23*, 1671−1676.
(72) Gans, P.; Buisson, G.; Duée, H.; Marchon, J.-C.; Erler, B. S.; Scholz, W. F.; Reed, C. A. *J. Am. Chem. Soc.* **1986**, *108*, 1223−1234.
(73) Inniss, D.; Soltis, S. M.; Strouse, C. E. *J. Am. Chem. Soc.* **1988**, *110*, 5644−5650.

a series of $[Fe(TArP)(CN)_2]^-$ complexes; replacement of the *meso*-2,4,6-trialkylphenyl groups by the *meso*-2,6-dichlorophenyl groups has changed the electron configuration from $(d_{xz}, d_{yz})^4(d_{xy})^1$ to $(d_{xy})^2(d_{xz}, d_{yz})$.[43]

We have mentioned in the previous section that the contribution of the $(d_{xz}, d_{yz})^4(d_{xy})^1$ state in bis(CN^-) and bis(HIm) complexes increases in the following order:

$$\text{OETPP} \leq \text{OMTPP} \leq \text{TPP} < \text{T}^n\text{PrP}, \text{T}^c\text{PrP} < \text{T}^i\text{PrP}$$

The larger contribution of the $(d_{xz}, d_{yz})^4(d_{xy})^1$ state in TRP complexes than in TPP complexes could be ascribed, to some extent, to the electron donating ability of the alkyl groups. Therien and co-workers have recently reported that bis(pyridine) complex of [*meso*-tetrakis(heptafluoropropyl)porphyrinato]-iron(III) shows a quite pure $(d_{xz}, d_{yz})^4(d_{xy})^1$ electron configuration.[66] The g_x, g_y, and g_z are 2.07, 2.07, and 1.99, respectively. Thus, the $|\Delta/\lambda|$ reaches as much as 26.4. Heptafluoropropyl group is bulky and electron withdrawing. Thus, two opposing factors are operating in this complex. Obviously, much more examples are necessary for the complete understanding of the electronic effect of peripheral substituents on the ground-state electron configuration of low-spin iron(III) porphyrin complexes.

Conclusion

Combined analysis of the ^{1}H and ^{13}C NMR chemical shifts and EPR *g* values have revealed that the highly saddle shaped $[Fe(ORTPP)(CN)_2]^-$ (R = Me and Et) has the common $(d_{xy})^2(d_{xz}, d_{yz})^3$ ground state. This contrasts to the ruffled $[Fe(TRP)(CN)_2]^-$ (R = ^{n}Pr, ^{c}Pr, and ^{i}Pr) which adopt the less common $(d_{xz}, d_{yz})^4(d_{xy})^1$ ground state. The difference in electronic ground state is explained in terms of the weaker $a_{2u}-d_{xy}$ and stronger $3e_g-d_\pi(d_{xz}, d_{yz})$ interactions in the saddle shaped $[Fe(ORTPP)(CN)_2]^-$ than in the ruffled $[Fe(TRP)(CN)_2]^-$. Replacement of CN^- by HIm further destabilizes the d_π orbitals, since the π-accepting ability of imidazole is weaker than that of cyanide. Thus, even $[Fe(T^nPrP)(HIm)_2]^+$ and $[Fe(T^cPrP)(HIm)_2]^+$ have shown the common $(d_{xy})^2(d_{xz}, d_{yz})^3$ ground state. In contrast, all the bis(^{t}BuNC) complexes examined in this study have shown the less common $(d_{xz}, d_{yz})^4(d_{xy})^1$ ground state. The contribution of the $(d_{xz}, d_{yz})^4(d_{xy})^1$ state to the electronic ground state differs, however, from complex to complex. On the basis of the ^{13}C NMR chemical shifts of *meso* carbons and EPR *g* values, it is concluded that the $(d_{xz}, d_{yz})^4(d_{xy})^1$ character increases in the following order: OETPP < OMTPP, TPP < T^nPrP, T^cPrP, T^iPrP. The similar order is established for the bis(CN^-) and bis(HIm) complexes: OETPP ≤ OMTPP ≤ TPP < T^nPrP, T^cPrP < T^iPrP. The smaller contribution of the $(d_{xz}, d_{yz})^4(d_{xy})^1$ state in the OETPP complexes than in the OMTPP complexes is explained in terms of the rigidity of the OETPP core; $[Fe(OETPP)(^tBuNC)_2]^+$ requires much larger energy for ruffling than $[Fe(OMTPP)(^tBuNC)_2]^+$ to stabilize the $(d_{xz}, d_{yz})^4(d_{xy})^1$ ground state. In the complexes with the a_{1u} porphyrin HOMO such as $[Fe(OEP)(^tBuNC)_2]^+$ and $[Fe(ProtoIXMe_2)(^tBuNC)_2]^+$, the contribution of the $(d_{xz}, d_{yz})^4(d_{xy})^1$ state is as small as that in $[Fe(OETPP)(^tBuNC)_2]^+$. Similarly, the complexes with electron withdrawing substituents at the *meso* positions such as $[Fe(F_{20}\text{-TPP})(^tBuNC)_2]^\pm$ have shown the smaller contribution of the $(d_{xz}, d_{yz})^4(d_{xy})^1$ state. On the basis of these results, we have concluded that the low-spin Fe(III) complexes having (i) strong σ-donors such as HIm, (ii) highly S_4-saddled porphyrin rings such as OETPP, (iii) porphyrins with a_{1u} HOMO such as OEP, and (iv) porphyrins with electron withdrawing substituents at the *meso* positions such as F_{20}-TPP, resist switching the electronic ground state from the common $(d_{xy})^2(d_{xz}, d_{yz})^3$ to the less common $(d_{xz}, d_{yz})^4(d_{xy})^1$.

Acknowledgment. The authors thank Prof. Hiroshi Kihara of Tokoha University for useful suggestions on the orbital interactions. This work was supported by the Grant in Aid for Scientific Research on Priority Areas(A) (No 12020257 to M.N.) from Ministry of Education, Culture, Sports, Science and Technology, Japan. T.I. is grateful to the JSPS Research Fellowship for young scientists. Thanks are due to the Research Center for Molecular Materials, the Institute for Molecular Science (IMS).

Supporting Information Available: Curie plots of the pyrrole protons and pyrrole-CH(α) protons in $[Fe(TRP)L_2]^\pm$ (R = ^{i}Pr, ^{c}Pr, ^{n}Pr), $[Fe(TPP)L_2]^\pm$, $[Fe(F_{20}\text{-TPP})L_2]^\pm$, and $[Fe(ORTPP)L_2]^\pm$ (R = Me, Et). This material is available free of charge via the Internet at http://pubs.acs.org.

IC001412B